ISSN 0736-5306

SCIENCE OF TSUNAMI HAZARDS

The International Journal of The Tsunami Society

Volume 15 Number 1 1997

OBJECTIVE: **The Tsunami Society** publishes this journal to increase and disseminate knowledge about tsunamis and their hazards.

DISCLAIMER: Although these articles have been technically reviewed by peers, **The Tsunami Society** is not responsible for the veracity of any statement, opinion or consequences.

Submit manuscripts of articles, notes or letters to the Editor. If an article is accepted for publication the author(s) must submit a camera ready manuscript in the journal format. A voluntary $50.00 page charge will include 50 reprints.

SUBSCRIPTION INFORMATION: Price per copy $20.00 USA

ISSN 0736-5306

Published by The Tsunami Society in Honolulu, Hawaii, USA

THE MINOR DESTRUCTIVE TSUNAMI OCCURRING NEAR ANTOFAGASTA, NORTHERN CHILE, JULY 30, 1995

Jorge Ramirez and Hernan Titichoca
Engineering Faculty
Universidad de Antofagasta
Antofagasta, Chile

James F. Lander and Lowell S. Whiteside
University of Colorado/CIRES
Boulder, CO 80309 USA

ABSTRACT

A destructive magnitude 8.1 Mw earthquake occurred near Antofagasta in northern Chile on July 30, 1995, at 05:11:23.6 GMT, and generated a moderate tsunami which was recorded by three local marigraphs. The maximum peak-to-trough height of the tsunami was 280 cm at Antofagasta, with a maximum runup of 245 cm measured at Caleta Blanco and 244 cm runup at La Rinconada Place. The tsunami caused US$131,200 in damage which included the submergence of four fishing vessels and damage to twelve others along with some damage to the wharf. The teletsunami was widely recorded around the Pacific Basin including a 2-3 m wave at Tahauku Bay, Hiva Oa in the Marquesas Islands which sank two small boats (Schindele, 1996; Guibourg, et al., 1997). Although the damage and casualties were relatively slight, the tsunami could have been disastrous had it occurred during daytime and in the summer when the beach is heavily utilized. The tsunami occurred on a winter night when the high tide had already fallen as much as 30 cm. The earthquake also caused damage, unrelated to the tsunami, to 120 homes and buildings in Antofagasta, Taltal, Mejillones, Calama, San Pedro de Atacama, and Tocopilla. Two fatalities, 58 injuries, and 630 homeless were reported. While reporting of moderate tsunamis is often incomplete, investigation of this type of tsunami is useful in order to better understand the mechanisms which cause tsunamis and the factors affecting runup in the area--in this case, an area which has not suffered a disastrous tsunami in its 391 years of recorded history.

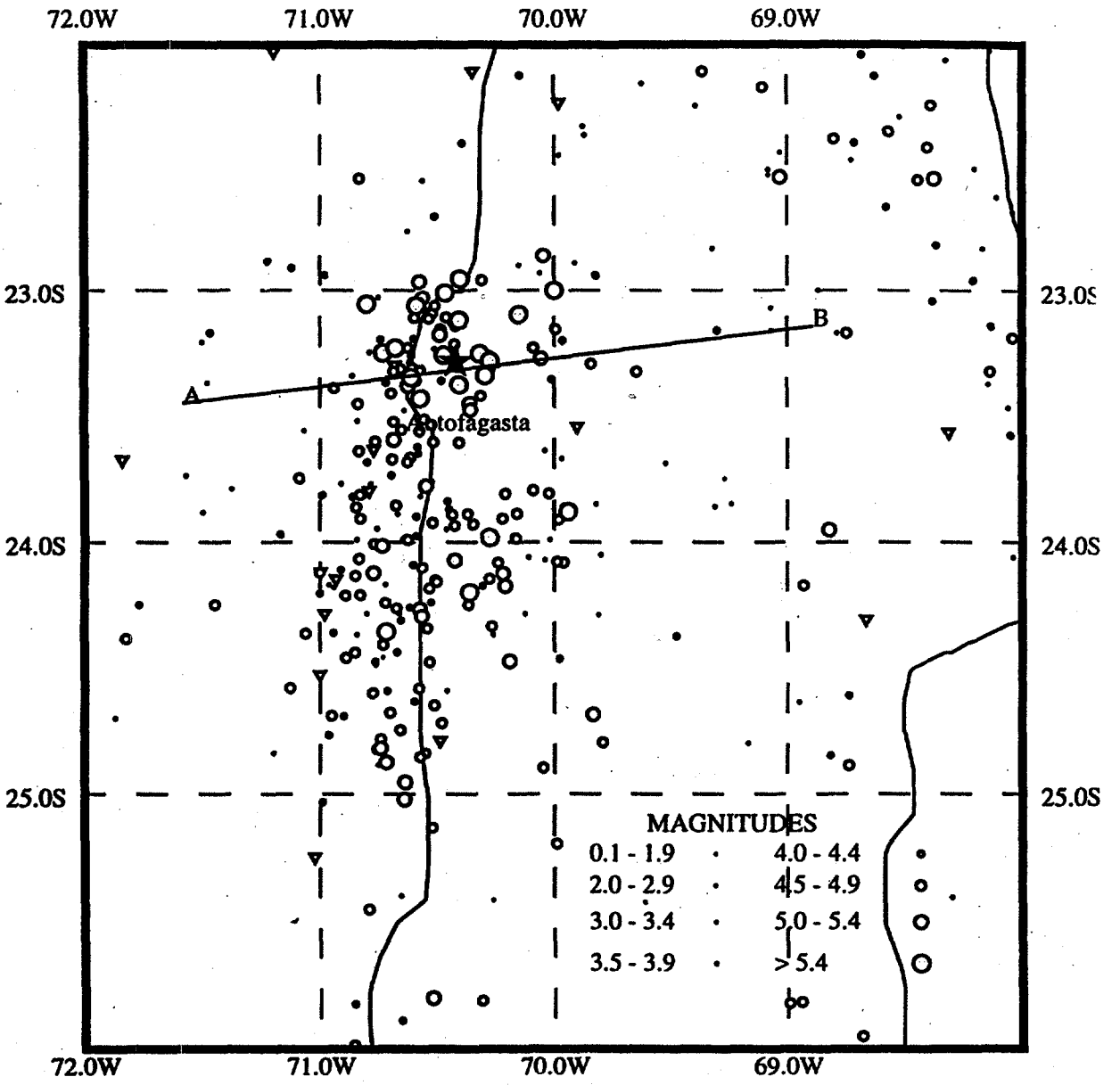

Figure 1. Locations of the 347 aftershocks (of all magnitudes) of the July 30, 1995 earthquake through December 1995, outlining the plate boundaries.

INTRODUCTION

On July 30, 1995, a violent earthquake occurred whose epicenter at 23.43S 70.48W (Ruegg, et al., 1996) was near Antofagasta, Chile. The earthquake at 05:11:23.6 GMT (1:11 a.m. local time), registered 8.1 Mw (Ruegg, et al., 1996) at a focal depth of 36 km (Monfret, et al., 1995). This was 2 hours and 45 minutes after high tide and the peak tide had subsided about 30 cm. In the next six months, 275 aftershocks of Mb 3.5 or above were located, characterizing a thrust zone extending from approximately 23 to 25 degrees South and from the oceanic trench, defining the boundary between the South American and Pacific plates, to about 70 to 71 degrees West longitude on shore (Figure1). The focal depths ranged from 22 km at the western end to 314 km at the eastern end towards the Andes, with an average angle of subduction of about 25 degrees (Figure 2).

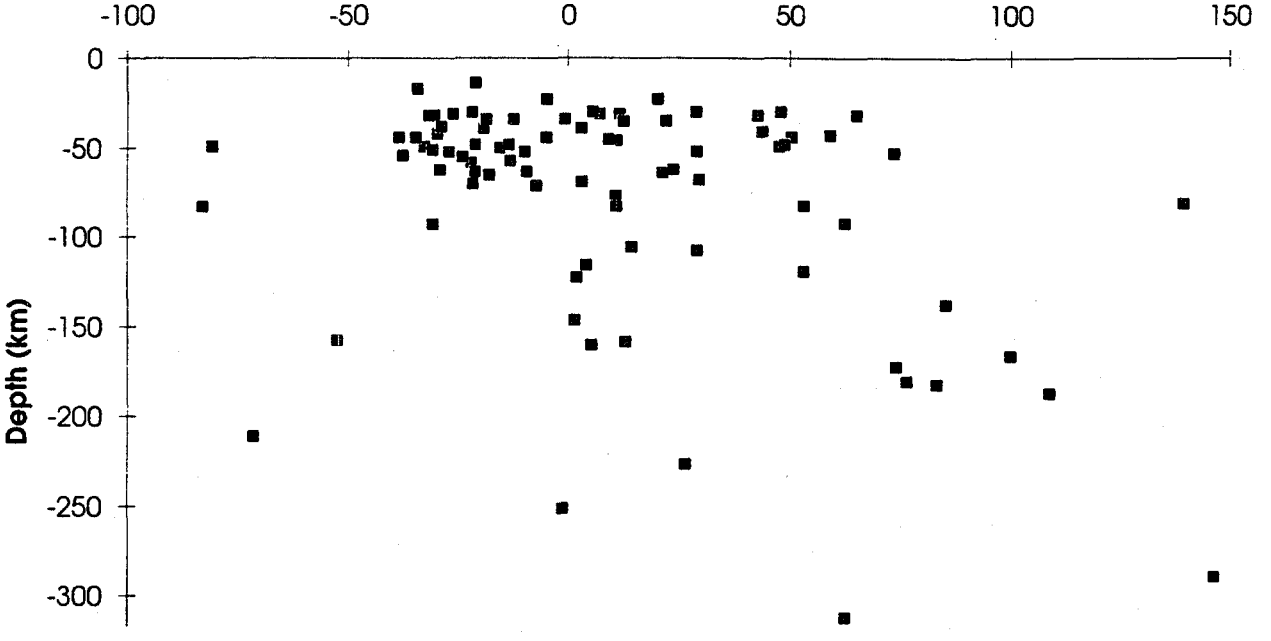

Figure 2. Cross-section of hypocenters projected within 100 km of line AB on Figure 1, perpendicular to the strike of the mainshock of July 30, 1995 (N75W), showing a dip of the zone of deformation of about 25 degrees to the east. Horizontal distance refers to distance along the line of projection from the epicenter.

This was the largest earthquake since the Ms 8.0 Taltal earthquake of Dec. 28, 1966, which occurred in an area slightly south of this rupture zone, and also produced a 45 cm tsunami at Antofagasta. With the possible exception of an intermediate-depth event on Dec. 9, 1950, several hundred kilometers inland, there are no historic records of a great (M>=8.0) earthquake in this section of the South American subduction zone. This earthquake, therefore, partially fills a seismic gap previously identified by Nishenko (1985).

The available tsunami history of the region (Figure 3), which begins with a questionable tsunami reported for November 19, 1873, is incomplete. Undoubtedly there must have been at least some earlier events in the nearly 400-year history which were not reported. This could possibly indicate that early tsunamis did not cause extensive damage, thus supporting the concept that the local source conditions in the region are not conducive to the generation of large local tsunamis. Tsunamis from outside the local area, as defined by the 1995 event, are somewhat more likely to cause damage. The largest wave reported in the literature for Antofagasta is from the May 9, 1877 Iquique event. This earthquake, to the north of Antofagasta, reportedly produced 6 m waves which caused extensive damage to homes and shops at Antofagasta. The August 13, 1868 Arica event and the March 22, 1960 southern Chile events did not produce waves at Antofagasta as large as the July 30, 1995 event, nor did they cause damage.

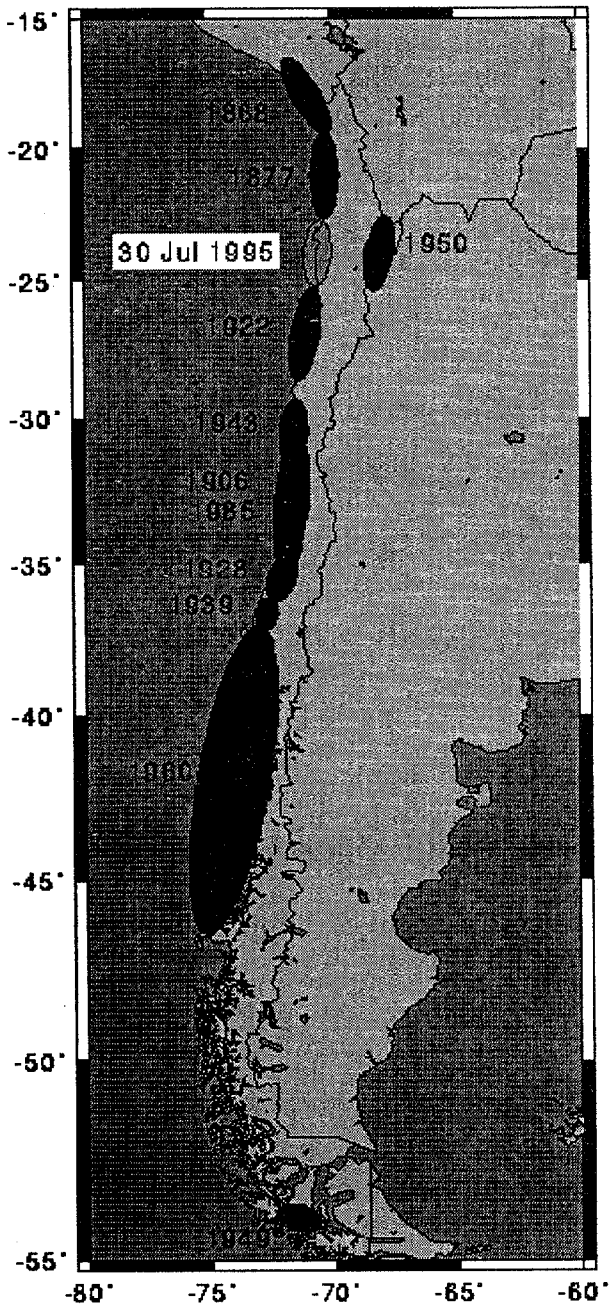

The resulting teletsunami was reported widely throughout the Pacific Basin (Figure 4). It was observed as a two- to three-meter wave at Tahauku Bay, Hiva Oa in the Marquesas Islands over 7000 km away, where two small boats were sunk by the second wave at three meters high behind the breakwater which inundated 250 m up the Tahauku River flooding 40,000 m^2 (Guibourg, et al.,1997). It was recorded with a 75 cm height at Hilo, Hawaii, and was likely recorded at a number of other sites which did not report to the Pacific Tsunami Warning System or the International Tsunami Information Center, the primary sources reports on Pacific-wide wave heights. Table I (appended at the end) shows tsunami heights from around the Pacific Basin in centimeters.

Figure 3. Location of historical Chilean earthquake rupture zones showing seismic gap filled by the July 30, 1995 earthquake. Illustration from Universidad de Chile at *http://www.dgf.uchile.cl/anto/rupt_mapa.html*

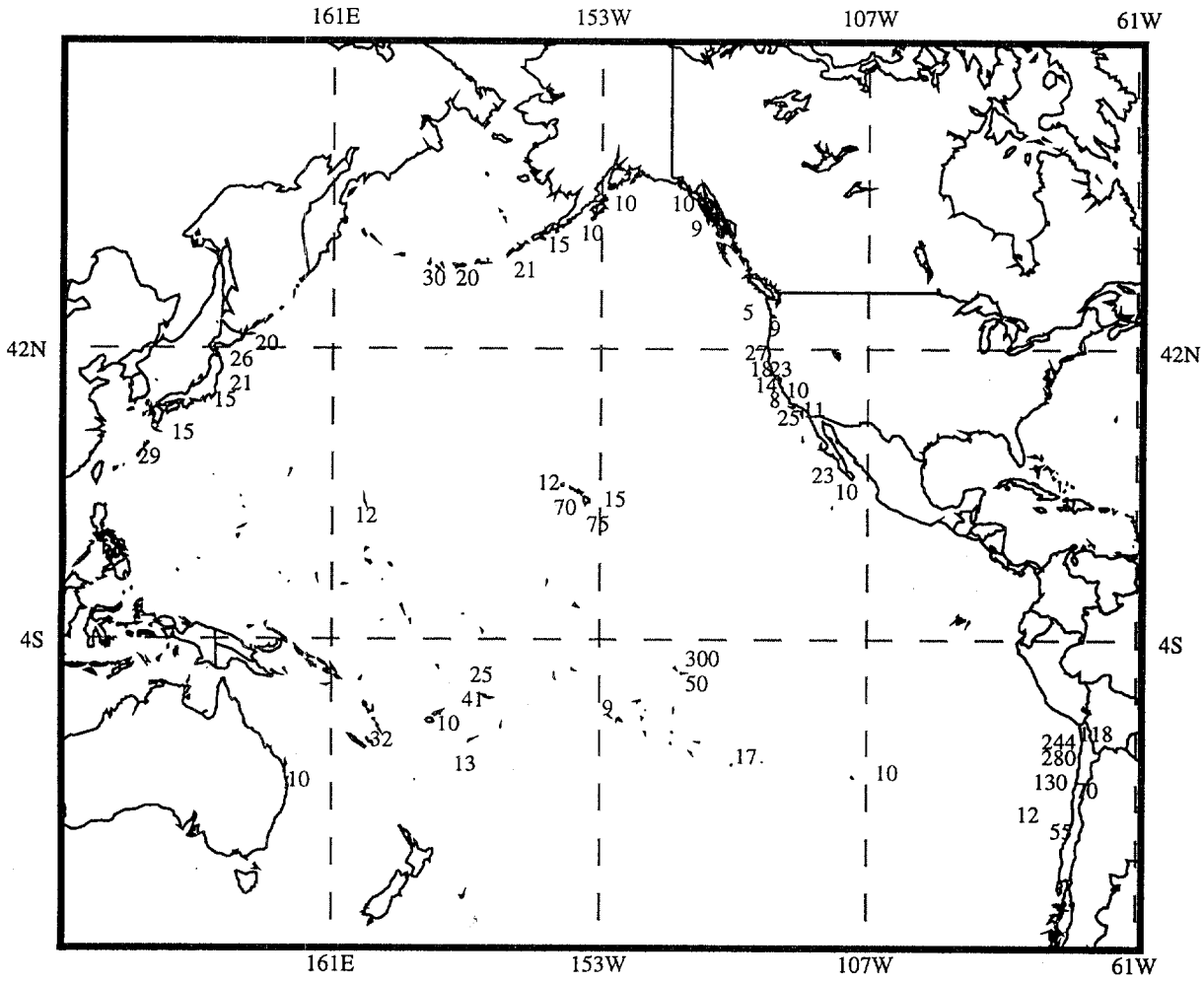

Figure 4. Selected teletsunami heights (peak-to-trough) from July 30, 1995 Antofagasta event in centimeters. Note the 300 cm height at Tahauku Bay, Hiva Oa in the Marquesas Islands and the 75 cm height at Hilo, Hawaii.

The efficiency in producing measurable waves at great distances around the Pacific from a moderate local tsunami may be the result of: 1) the somewhat steep subduction angle (Ruegg, et al., 1996), 2) the geometry of the trench, or 3) the sea bottom slope at the source coast, which may reflect a greater portion of the energy away from the local coast.

In spite of the powerful earthquake, damage to buildings was not very extensive. A total of 120 houses and buildings were damaged in Taltal, the main city of Antofagasta with a population of 250,000, and Mejillones as well as in Calama, San Pedro de Atacama, and Tocopilla (Figure 5). Only two people died as a result of the earthquake. This small effect from such a powerful earthquake may be due to a reduced intensity due to the depth of focus of the subduction zone on land which was between 90 and 300 km. According to Olivares and Toro, 1995, intensities of earthquakes in this area historically do not generally exceed VIII on the Modified Mercalli Intensity Scale (MMI). The notable exceptions are the earthquakes of April 22, 1870, and Nov. 3, 1933, both of which were significantly more destructive and registered X MMI.

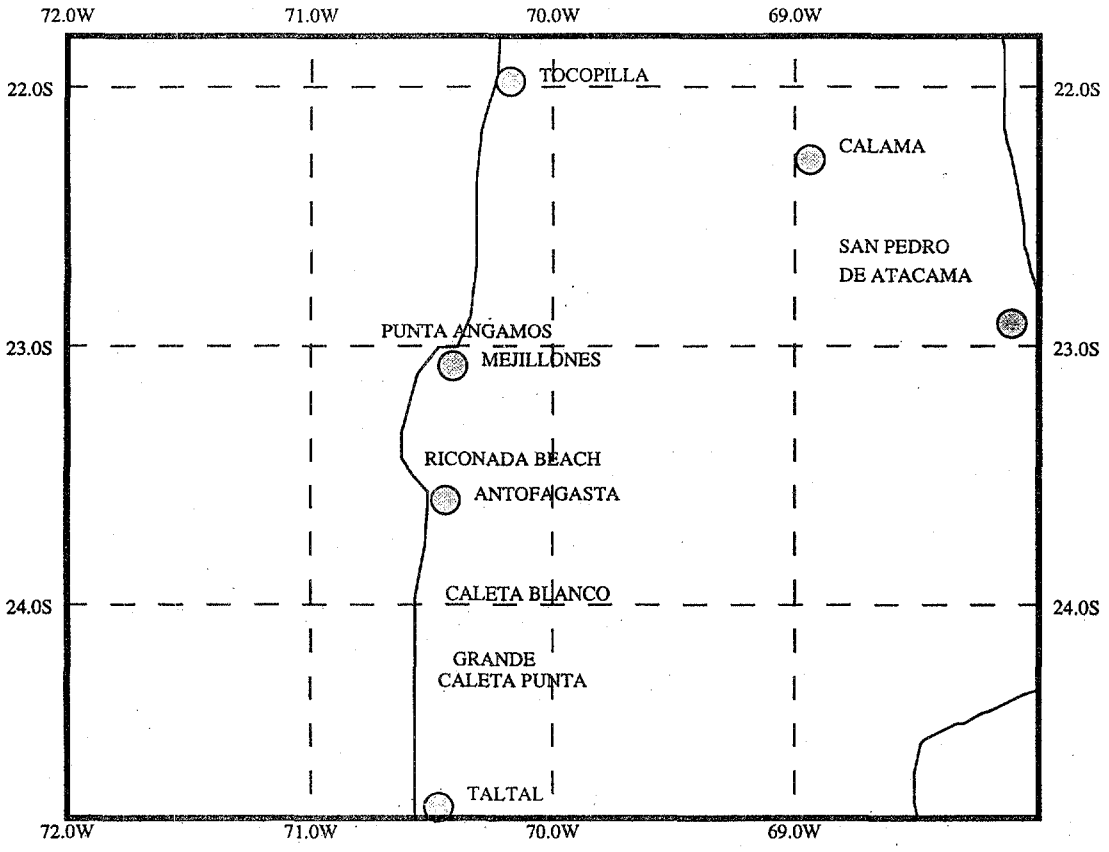

Figure 5. Location map for area affected by the earthquake and local tsunami of July 30, 1995 event.

This earthquake generated only a small tsunami causing relatively minor damage including the submergence of 4 fishing vessels, damage to 12 others, and some damage to docks totaling damages of US$131,200.

DATA

Marigrams were collected from three local instruments located, from north to south, at 1) Punta Grande Bay operated by Sociedad de Estudios Ambientales (SEARCH), 2) the port of Antofagasta, and 3) the thermoelectric plant of Codelco in the city of Tocopilla. Two other measurements of note, obtained from direct topographic instrument measurements of the maximum runup, were at Caleta Blanco and at La Rinconada Place. La Rinconada Place is located on the eastern coast of Mejillones Peninsula, northwest of Antofagasta where the height was 244 cm and the inundation reached 239 m, flooding the road to Juan Lopez Beach. Figure 6 shows the elevation cross-section and Figure 7 shows the inundation at La Rinconada Place. Marigraphic and topographic measured heights and beach slopes are given in Table II.

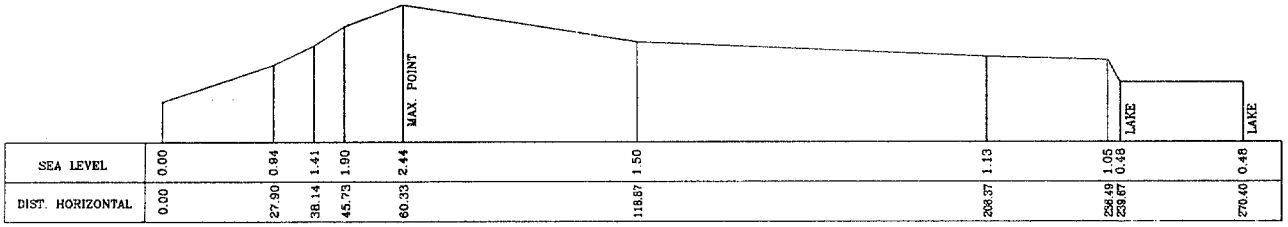

Figure 6. Elevation cross-section of runup and inundation at La Rinconada Place on July 30, 1995 at Antofagasta, Chile.

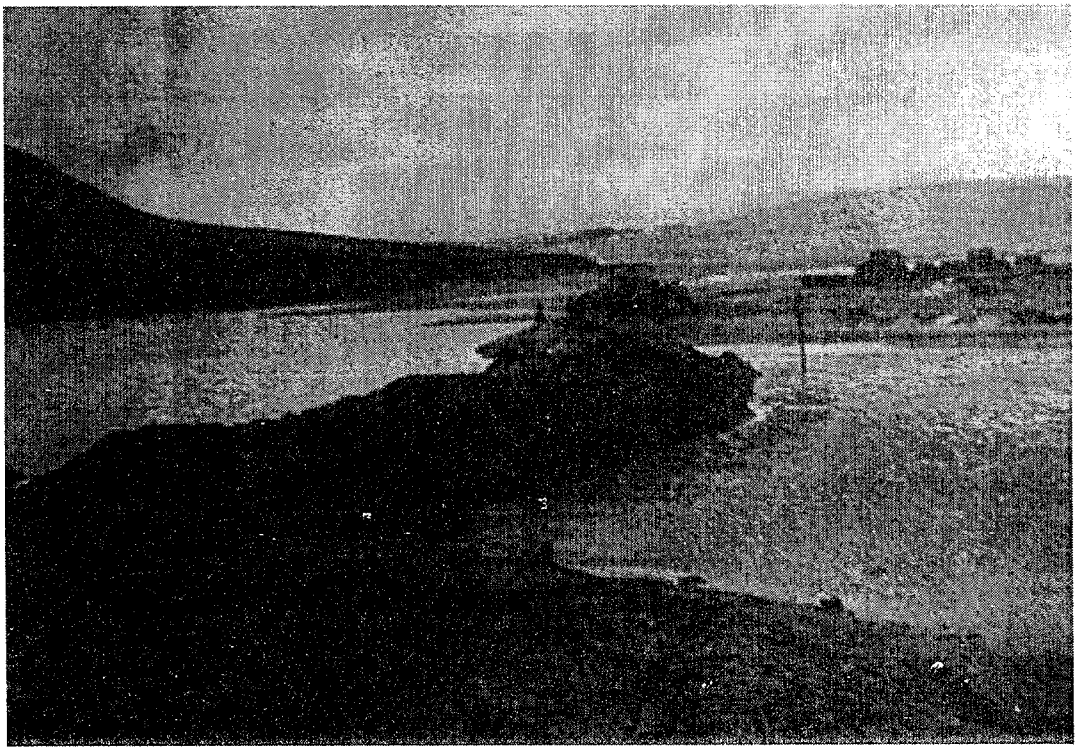

Figure 7. Photograph of the inundation at La Rinconada Place.

The Universidad de Antofagasta ship, *Purihalar,* was anchored in Caleta Bay. Capt. Carlos Guerra Correa reported that a few minutes after the earthquake the ship's echo sounder showed changes in depth ranging from 1.5 to 11 m of water below the ship's keel. Although the ship swinging on its anchor was not damaged, they were fearful that the ship would run aground. The GPS instruments recorded movements like "figure eights." The shallower depths would have occurred near shore during the height of the incoming tsunami, while the deeper measurements would have been during the withdrawal stage.

Interviews with observers and subsequent investigations showed that the sea reached a level of 245 m at a small peninsula of Punta Cangrejos, cutting it off from the mainland and leaving it as an island at times. Several fishermen were temporarily trapped on the point until the sea receded. The first reaction of the fishermen was to escape. The distance to escape was 30 to 40 m, so the sea probably invaded the area in no more than two minutes. The guard of the Yacht Club at Antofagasta, who observed the motion of the sea, reported that, just as the earthquake finished, the water was quiet for seven minutes and then began to drop. There was a loud noise for about 10 minutes. Afterward the sea motion continued for several cycles. The report that the water level first fell is not supported by the marigrams. It is not uncommon for the withdrawal to be the first motion noticed when the true first movement is a rise. The initial rise is an amplitude and the withdrawal is a height which is twice as large. The withdrawal often drags shells and pebbles with it creating a noise.

Figure 8. One of the fishing boats being rescued in Antofagasta's fishing port and yacht club of the type damaged or sunk by the tsunami.

Seismic data from the mainshock were obtained from the United States Geological Survey's (USGS) National Earthquake Information Service (NEIS), Harvard's focal mechanisms, the International Data Center (GSETT), the University of Chile, and other sources. Reports of amplitudes at marigraphic stations around the Pacific were gathered from the International Tsunami Information Center (NTIC).

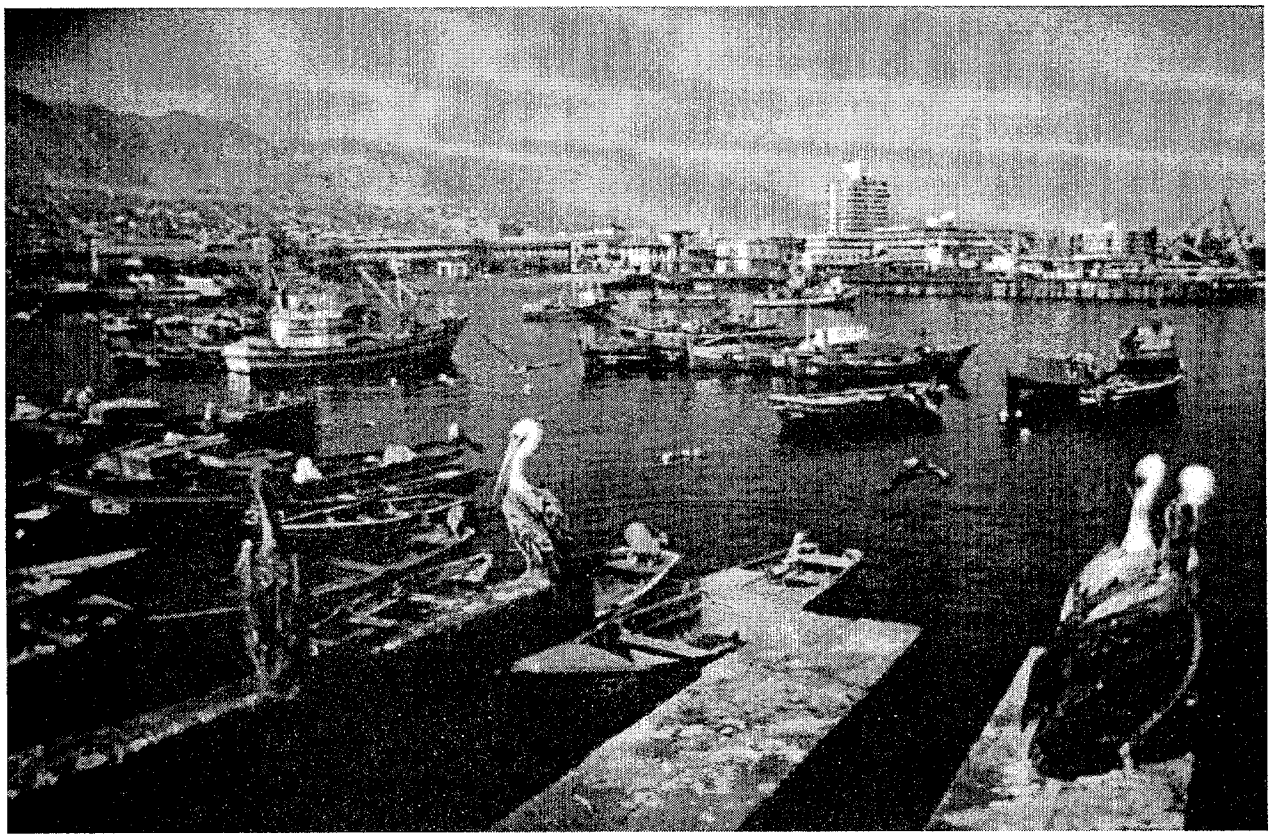

Figure 9. The small fishing port and yacht club at Antofagasta.

The mainshock was a shallow underthrusting event with a strike of N25E and a dip of 25 degrees (Harvard Centroid Moment Tensor Solution). The USGS alternatively found a strike of N5W and a dip of 19 degrees. The second set of values seems more plausible in terms of the trend and plunge of the trench at this locality. Ruegg, et al., (1996) have modeled the quake based on Very Broad Band (VBB) digital records and confirm the USGS dip but find a strike of N8E, more consistent with the strike of the trench. The mainshock is placed from 57 to 32 km depth by the various sources. None of the aftershock epicenters were located at depths less than about 20 km. There were no surface breaks reported on land. Aftershocks with depths greater than 110 km are few and irregularly located. This suggests that deeper aftershocks were not on the rupture plane, but represented quakes caused by redistribution of stress from the mainshock. It is often noted that aftershocks avoid the rupture plane and cluster in the surrounding materials, since the rupture relieves most or all stress on the plane itself.

The magnitude of the event is variously reported as Ms 7.5 (GSETT), Ms 7.6 (USGS), and Mw 8.1 (Ruegg, et al., 1996). Because of the careful study done in obtaining this magnitude, we tend to prefer the Mw 8.1 value. The epicenter is located consistently by all reporters at about 23.4S 70.5W.

Information on damage was gathered from official sources in Antofagasta. The primary tsunami damage was the submergence of four fishing boats and damage to 12 others. This was due mainly to the strong currents created by the rapid rise and fall of the water level. These currents

caused the boats to break free from their moorings and collide with other boats as well as the dock. Figure 8 shows a boat of the type damaged or sunk being recovered. Figure 9 shows the small fishing port and Yacht Club where most of the damage occurred.

Figure 10 shows the north beach at Punta Cangrejos where the maximum height levels and inundated areas reached by the sea were measured with precision topographic instruments. The traces of a lake created temporarily by the tsunami can be seen. The point was completely cut off from the mainland temporarily trapping several fishermen.

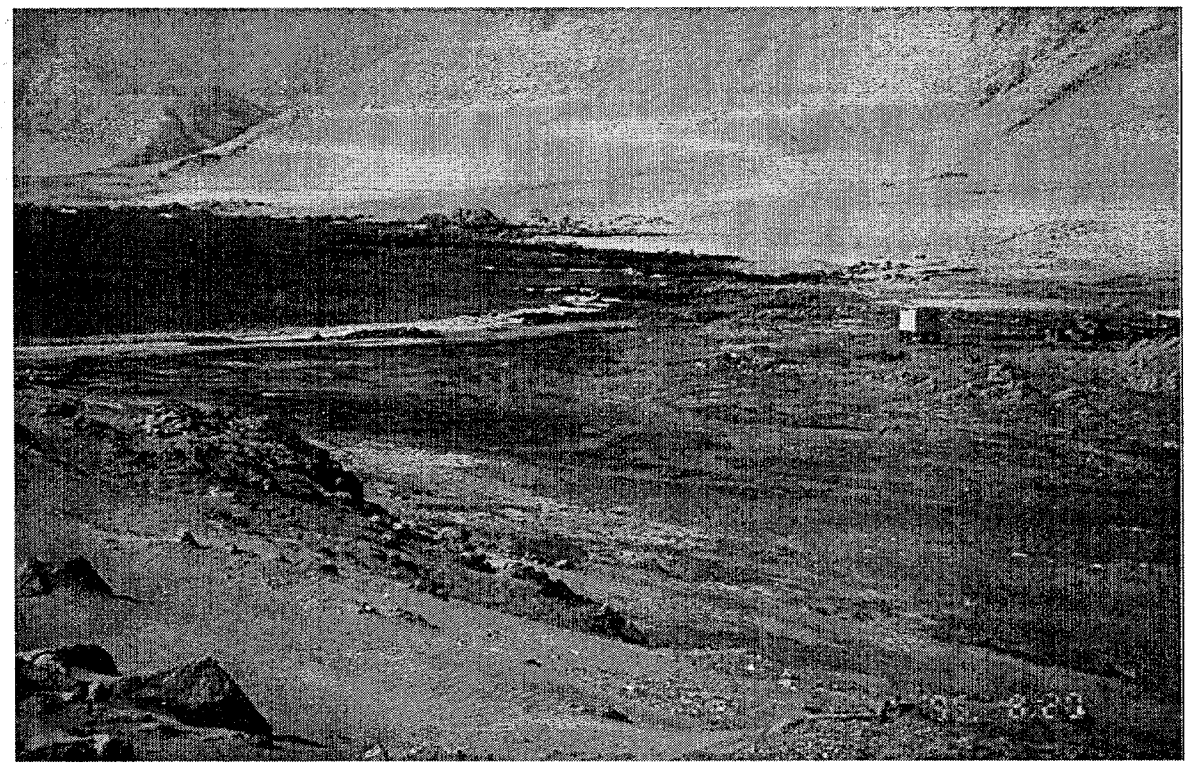

Figure 10. The north shore of Punta Cangrejos where the tsunami cut across the 245 meter wide point creating an island at times and trapping temporarily several fisherman. The traces of a new temporary lake can be seen. This was the place where maximum inundation occurred.

DISCUSSION

In December 1994, a thesis was finished by Olivares and Toro, to obtain their Agrimensor [Surveyor] Engineering degree, entitled "Seismic Hazard in Antofagasta," under the guidance of Prof. Jorge Ramirez Fernandez at Universidad de Antofagasta, Chile. Some of the conclusions included in this work are relevant for the present paper. First, the main threat, in terms of the expected intensity of the horizontal acceleration of ground motion for the city of Antofagasta, would come from an earthquake generated in an area near the city, in a radius less than 100 km, as has historically been the case. This would put the epicenter within the tectonic block defined by the aftershocks of this earthquake. It is apparent that if a great earthquake in the northern part of Chile

or southern part of Peru should occur, regardless of magnitude, the intensity should not exceed VII MMI. This is due to the soil of Antofagasta and the distance that separates these two great epicenters from the city of Antofagasta--more than 400 km--which would attenuate the seismic waves sufficiently so that they would not be destructive. Secondly, if a great earthquake were to occur in the extreme northern part of Chile, although the seismic waves would not be particularly destructive, the possible tsunami could potentially affect many Chilean ports and coastal cities. These potential tsunamis would not only affect the Chilean coast in its totality, but also the coast of the whole Pacific Basin.

Historically, large tsunamis have been generated in the extreme northern and southern parts of Chile. The Mejillones Peninsula probably protected Antofagasta from this event. The 1868 Arica earthquake generated a tsunami with reported heights of 6 m at Mejillones, but the effects at Antofagasta, if any, are unreported in standard tsunami catalogs. The 1960 southern Chile earthquake produced a tsunami of 1.4 m peak to trough at Antofagasta. This was the situation for the area of Antofagasta presented by Olivares and Toro, prior to the occurrence of the July 1995 earthquake. Below, we compare the seismic hazard and risk predictions by Olivares and Toro with the damage and risk observations during and following the July 30, 1995 earthquake. Some observations were predicted while others were unexpected. Nevertheless, risk studies such as this contribute significantly to attempts to reduce damages and loss caused by the forces of nature.

THE TSUNAMIGENIC EARTHQUAKE OF JULY 30, 1995

On July 30, 1995, at 05:11:23.6 Universal Time, (01:11:23.6 Chilean time), the main earthquake with a magnitude (Mw) of 8.1 occurred. The epicenter, 23.43 S and 70.48 W, off shore with a depth focus of 32 km (Ruegg, et al., 1996), located near Antofagasta (Figure 1). The city of Antofagasta is located about 63 km from the main hypocenter and within the zone of rupture shown by the aftershocks. Four strong aftershocks followed a few minutes later. The first, at 05:22:52.9 GMT, occurred at the southernmost section of the rupture with Ms 7.1 (GSETT). The second, at 05:26:35.9 GMT (Ms 6.9) was located in the center of the peninsula of Mejillones, 40 km inland to the north of the city. The third (Mb 5.9) was near the epicenter at 05:47:01.4 GMT. The fourth (Mb 5.4) occurring at 05:50:03.1 GMT, was located about 50 km east of the mainshock in the Cordillera de La Costa, 97 km north east of the city of Antofagasta. In addition, approximately 350 minor earthquakes followed, which were located along a great extension of the coastal zone, from the peninsula of Mejillones to Paposo in the Chilean Administrative Region II. The aftershocks coincided with the strike of the subduction of the Nazca plate along a distance of more than 160 km.

The largest aftershocks occur 11 min 30 sec (Ms7.1 GSETT), 15 min 18 sec (Ms6.9 GSETT), 35 min 45 sec (Mb 5.9), and 38 min 46 sec (Mb 5.4) after the mainshock. These aftershocks may have been triggered at sites of high strain concentration by the arrival of reflected seismic phases ScP, ScS, SKKP, SKKS which return to the epicentral region at these respective times (Whiteside and Ben-Zion, 1995).

It has been noted previously, in the study of seismic risks for the city of Antofagasta, that earthquakes which are very close to the city can generate destructive accelerations on the rocky soil of the city, causing damage. This was also the case with this event. The major earthquake accelerated the rock soil horizontally approximately 132 cm/sec2. This is equivalent to the

beginning of intensity VIII MMI. The main wave was considerably attenuated in acceleration due to the top of the subducting plate being more than 100 km beneath Antofagasta.

In summary, we observe that the major earthquakes of the extreme northern part of Chile do not exceed the accelerations and intensities at Antofagasta of the smaller earthquakes that are closer. Therefore, they represent relatively minor threats.

On the contrary, historically, the main hazard from earthquakes in northern Chile is not due to local shaking from the earthquake but rather to the major tsunamis generated by these earthquakes. These tsunamis affect both national and pan-Pacific coastlines. In consequence, the real hazard of an earthquake generated in the extreme northern part of Chile is the possibility of a destructive tsunami.

The earthquake of July 1995, supports the history of almost 400 years of non-destructive, local tsunami occurrence, generated in this part of the Chilean coastal territory. Approximately 24 tsunamis have been reported as originating between the latitudes 20 and 26 south. Because of the relatively small size of blocks in this region of Chile, the earthquakes tend to be smaller. Smaller earthquakes displace less water and generally, if a tsunami is generated, it is non-destructive. This must only be understood as a historical tendency observed during approximately 400 years. It does not ensure that it has not occurred before nor that it will not occur in the future.

THE MINOR DESTRUCTIVE TSUNAMI OF JULY 30, 1995

No fatalities or injuries resulted from this tsunami, but there was minor damage. Since it occurred at 01:11 on Sunday July 30, the majority of the small boats and vessels were anchored at fisherman wharves. Also, since it was wintertime, no people were sleeping on the beaches or at beach resorts, which was very fortunate. If this tsunami had occurred during the summertime and during the day, the resulting damage and casualties probably would have been significantly more extensive.

Recordings from the three marigraphs (Figure 11) allowed us to determine the times of arrival, periods, and the relative heights of the tsunami. Marigraphs usually record lower heights than the true wave due to their damping of higher-than- tidal periods. However, surveys of runup at Antofagasta port support the recorded height. Observations from two other sites (also noted above) as well as instruments and reports of the crew of the Universidad de Antofagasta oceanographic ship, *Purihalar*, anchored in that small bay that morning, in the epicentral area (Figure 2), were also used to measure the tsunami.

CONCLUSIONS

1. The first motion of each marigram showed an elevation of the sea level. This indicates that the disturbance generated by this earthquake was an uplift of the ocean surface perhaps due to thrusting of the oceanic plate. This could have been caused by an uplift of the ocean bottom or by a thrusting of the oceanic plate into the trench. This is confirmed by the reports of the geophysical scientists (Ruegg, et al., 1996), that indicate a maximum elevation of 40 cm near Mejillones Peninsula, measured with GPS of the continental surface. This also could have been caused by motion of the continental plate with respect to the subducting oceanic plate which was measured motion of 86 cm to the southwest by the South American Geodynamic Activities (SAGA) project near Antofagasta, and could have been much larger in the trench.

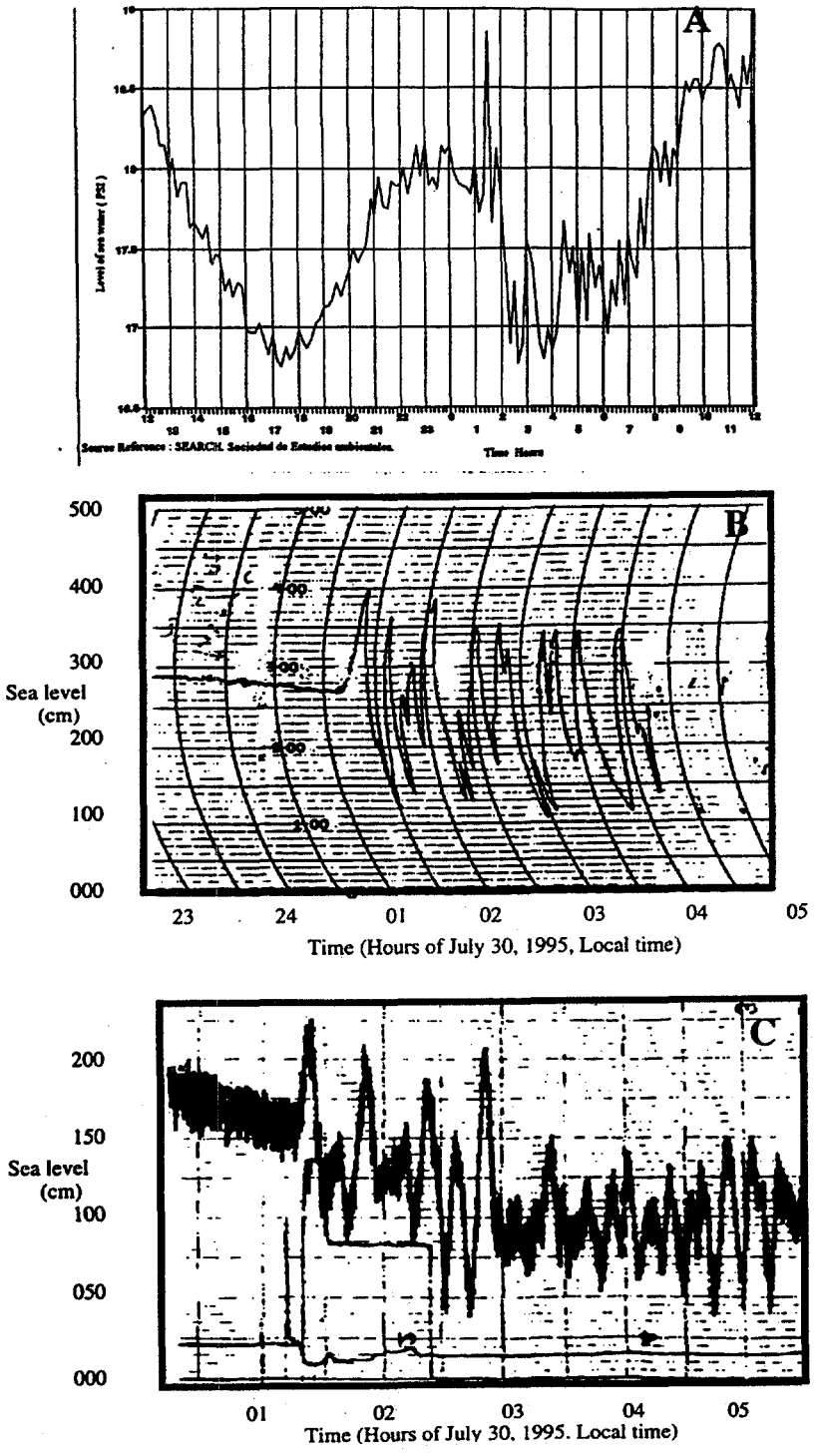

Figure 11. Local marigrams from the July 30, 1995 tsunami. A. Punta Grande Bay; B. Antofagasta Port; C. Thermoelectric Plant, Tocopilla.

2. The marigrams indicate the time of arrival of the tsunami at the different stations. The time of the origin of the initiation of the rupture is available as the earthquake origin time. It would take about 37 seconds for the rupture to reach the trench traveling at the S-wave velocity (~3.5 km/sec). At this point the tsunami would be generated. To reach shore at Antofagasta, the tsunami would travel 120 km. This would take about 9.14 minutes, estimating an average velocity of 787 km/hr. Calculated times to Tocopilla and Caleta Blanco are respectively 15 minutes and 9 minutes. It reportedly took 14 minutes to reach Tocopilla, 4 minutes to reach Antofagasta, and 2 minutes to reach Caleta Blanco. These travel times, if accurate, indicate a source offshore between for Antofagasta and Caleta Blanco, but modeling of travel times does not define the source area well using the given travel times.. If correct, these results show that the time available for evacuations following the earthquake initiation would be a very short. A warning system would not have time to operate. The public would have to be educated to flee the coastal region at the onset of the earthquake.

3. The behavior of this tsunami was typically local, with the main inundation levels recorded in a radius less than 250 km from the center of the aftershock area (Figure 1). The records indicate that, for Tocopilla, located 235 km north of the main epicentral area, the level was 70 cm higher than the normal corresponding level for that moment (Figure 11). Antofagasta reached 130 cm above the corresponding normal level for that moment. Caleta Blanco registered the highest runup of 245 cm, measured from the average sea level, since there is no marigraph record here. Finally, the marigraphic record of Caleta Punta Grande recorded an increase in the level of 80 cm. The area inundated, of course, would have been greater if the tsunami had occurred at high tide. Fortunately, it took place 2 hours and 45 minutes after the peak high tide as shown in the records. These higher levels would have been an average increase of 30 cm probably causing some destructive flooding.

4. Although the tsunami had a maximum local runup height of only 245 cm, it was observed widely around the Pacific. Pacific-wide observations included a 300 cm wave reported at Tahauku Bay, Hiva Oa in the Marquesas Islands, which sank two small boats and inundated 40,000 m^2 of land. A wave height of 75 cm was reported at Hilo, Hawaii, and measurable waves in Japan, Alaska, Australia, Mexico, and Samoa were also reported. The tsunami was probably recorded at many other locations as well.

5. The shape of the marine bottom near coasts can increase or decrease the inundation levels, since they may reflect or channel a proportion of the tsunami waves. The parameter that represents the steepness or flatness of the immersed beach next to the coast, is its slope. Investigating the available data of three close stations, you can observe the effect of the slope. For instance, it is clearly noticeable that the steep marine bottoms reflect more energy, while the flatter ones transmit more energy, allowing a higher level of inundation. It can be inferred that the shape of the beach can turn out to be a natural marine wall when it is steep. On the contrary, when it is flat, it increases the inundation levels of tsunamis, and therefore, it constitutes a risk element to consider.

ACKNOWLEDGEMENTS

The completion of this paper and its publication was supported by the National Science foundation Project CMS952369S for $208,815, to create a catalog of tsunamis occurring since 1982.

We appreciate the editing assistance provided by Karen Fay O'Loughlin, Cooperative Institute for Research in Environmental Sciences, University of Colorado, Boulder.

We would like to acknowledge the cooperation of the following agencies who provided marigrams:

- Chilean Navy, Marigraphic record of July 30, 1995, in the Port of Antofagasta.
- CODELCO Chile in Tocopilla, Marigraphic record of July 30, 1995, in the Thermoelectric Power Plant in Tocopilla.
- SEARCH, Environmental Studies Society, Tsunami record of July 29-30. 1995 in Punta Grande.

BIBLIOGRAPHY

Guibourg, S, P. Heinrich, and Roger Roche, 1997. Numerical modeling of the 1995 Chilean tsunami. Impact on French Polynesia, *Geophys. Res. Let.,* Vol.24, No. 7, pp. 775-778.

Klotz, Jurgen, 1996. "The SAGA Project: GPS derived deformation of the central Andes including the Mw = 7.6 Antofagasta earthquake," IV Congreso Internacional de Ciencias de la Tierra, Ponencias y Seminarios 05-09 Agosto de 1996, Instituto Geografico Militar de Chile, p. 223.

Lockridge, Patricia A., 1985. "Tsunamis in Peru-Chile," World Data Center-A for Solid Earth Geophysics, Report SE-39, National Geophysical Data Center, Boulder Colorado, U.S.A., 95pp.

Monfret, T., L. Dorbath, J.P. Caminade, M. Prado, D. Comte, L. Ponce, A. Cisternas. B. Delouis, and L. Rivera, 1995. "The July 30, 1995, Antofagasta earthquake: An 'hypocritical' seismic event," *EOS Transactions,* Vol. 76, No. 46, p. 427.

Nishenko, S.P., 1985. "Seismic potential for large and great intraplate earthquakes along the Chilean and southern Peruvian margins of South America: A quantitative appraisal." *J. Geophys. Res.,* Vol. 90. pp. 3589-3615.

National Earthquake Information Center, 1995. "Data bulletin of the earthquake of July 30, 1995, occurred in the coastal zone near the city of Antofagasta, Chile," Golden, CO, U.S.A.

National Earthquake Information Center, 1995. "Preliminary determination of epicenters," July Monthly Listing, US Geological Survey, Golden, CO, USA.

Olivares, Hector, and Daniel Toro, 1994. "The seismic hazard in Antofagasta," Thesis for Agrimensor Engineer, Engineering Faculty, Universidad de Antofagasta.

Ortlieb, L., S. Barrientos, A. Lavenu, and T. Monfret, 1995. "Coseismic uplift motion near Antofagasta, N. Chile, related to the July 30, 1995, Ms 7.3 event: First field evidence from the intertidal area," *EOS Transactions,* Vol. 76, No. 46, p. 375.

Ramirez, Jorge, and Titichoca, Hernan, 1995. "Three theoretical models of tsunami inundation applied to the cities of Arica and Iquique in contrast with the historical values," *Innovation Magazine,* Year 7, No. 1, May.

Ruegg, J. C., J. Campos, R. Armijo,S. Barrientos, P. Briole, R. Thiele, M. Arancibia, J. Canuta, T. Duquesnoy, M. Chang, D. Lazo, H. Lyon-Caen, L. Ortlieb, J. C. Rossignol, and L. Serrurier, 1996. "The Mw = 8.1 Antofagasta (north Chile) earthquake of July 30, 1995: First results from teleseismic and geodetic data," *Geophys. Res. Let.,* Vol. 23, No. 9, pp. 917-920.

Schindele, Francois, 1996. "Centre Polynesien Prevention des Tsunamis, new MO threshold for Tahauku Bay at Hiva Oa," *Tsunami Newsletter*, Vol. XXVIII , No. 1, p. 50.

Soloviev, S.L. and Ch. N. Go, 1975. "A catalogue of tsunamis on the eastern shore of the Pacific Ocean," Academy of Science of the USSR, Nauka Publishing House, Moscow, 204 pp. Translated in 1984, by the Canadian Institute for Scientific and Technical Information, National Research Council, Ottawa, Ontario, Canada, 285 pp.

Whiteside, L. and Y. Ben-Zion, 1995. "Universal triggering patterns in earthquake sequences and the use of triggering for earthquake prediction," *EOS Transactions,* Vol. 76, No. 46, p. 532.

TABLE I Tsunami Heights from Around the Pacific Basin in centimeters.

Country	Region	Reporting Location	Height in cm
Australia		Gold Coast	10
Chile		Antofagasta	280
		La Rinconada Place	244
		Caldera	130
		Punta Grande Place	118
		Tocopilla	70
		Valparaiso	55
		Juan Fernandez	12
		Easter Island	10
Fiji		Lautoka	10
French Polynesia	Gambier Islands	Mangareva, Rikitea	17
	Marquesas Islands	Hiva Oa, Tahauku Bay	300
		Nuku Hiva, Taiohae Bay	50
	Tahiti	Papeete	9
Japan	Bonin Island	Chichijima I	14
	Hokkaido Island	Hanasaki, Nemuro	20
	Honshu Island	Hachinohe	26
		Ayukawa	21
		Shionomisaki Cape	19
		Onahama	15
		Owase	15
		Choshi	15
		Omaezaki	14
		Hachijo I	9
		Oofunato	8
	Kyushu Island	Aburatsu	13
		Hyuga-Shirahama	13
		Tosashirahama	11
		Makurazaki	6
	Ryuku Island	Miyako	29
	Shikoku Island	Murotomisaki Cape	10
Mexico		Socorro Island	23
		Cabo San Lucas	10
Tonga		Nuku'alofa	13
USA	Hawaii	Hilo	75
		Kahului	70
		Honolulu	15
		Nawiliwili	12

TABLE II Tsunami Heights from Around the Pacific Basin in centimeters. continued

Country	Region	Reporting Location	Height in cm
USA (con't)	California	Crescent City	27
		Santa Monica	25
		San Diego	11
		Los Angeles	10
		Arena Cove	14
		Point Reyes	18
		Monterey	8
		Point San Luis	23
	Washington	Neah Bay	5
	Oregon	Port Orford	9
	Alaska	Adak	30
		Sand Point	21
		Shemya	20
		Dutch Harbor	15
		Sitka	10
		Kodiak	10
		Yakutat	10
		Seward	9
	Samoa	Pago Pago	25
	Wake Island		12
Vanuatu		Pt Vila	32
W. Samoa		Apia	41

Table II Marigraphic and Topographic Measured Heights and Beach Slopes.

Station Location	Water Height(cm)	Immersed Beach Slope (degrees)
Tocopilla (Marigraphic)	70 (peak to trough)	2.72
Antofagasta (Marigraphic)	260 (peak to trough)	2.26
Punta Grande (Marigraphic)	120 (peak to trough)	2.70
Caleta Blanco (Topographic)	245 (runup)	1.70
La Rinconada Place (Topographic)	239 (runup)	0.76

TABLE II Tsunami Heights from Around the Pacific Basin in centimeters. continued

Country	Region	Reporting Location	Height in cm
USA (con't)	California	Crescent City	27
		Santa Monica	25
		San Diego	11
		Los Angeles	10
		Arena Cove	14
		Point Reyes	18
		Monterey	8
		Point San Luis	23
	Washington	Neah Bay	5
	Oregon	Port Orford	9
	Alaska	Adak	30
		Sand Point	21
		Shemya	20
		Dutch Harbor	15
		Sitka	10
		Kodiak	10
		Yakutat	10
		Seward	9
	Samoa	Pago Pago	25
	Wake Island		12
Vanuatu		Pt Vila	32
W. Samoa		Apia	41

Table II Marigraphic and Topographic Measured Heights and Beach Slopes.

Station Location	Water Height(cm)	Immersed Beach Slope (degrees)
Tocopilla (Marigraphic)	70 (peak to trough)	2.72
Antofagasta (Marigraphic)	260 (peak to trough)	2.26
Punta Grande (Marigraphic)	120 (peak to trough)	
Caleta Blanco (Topographic)	245 (runup)	1.70
Rinconada Beach (Topographic)	239 (runup)	6.70

TSUNAMI WEB SITE DIRECTORY

A web site with the listing of all the papers published during the last 15 years of *Science of Tsunami Hazards* is being published by Dr. Antonio Baptista. The web site has the following URL:

http://www.ccalmr.ogi.edu/STH

Any author who wishes to have his entire paper on the web site should make arrangements with the web site publisher, Dr. Antonio Baptista at :baptista@ccalmr.ori.edu.

A web site about Tsunamis is being published by another **Tsunami Society** member, Dr. George Pararas-Carayannis. His tsunami web site has the following URL:

http://www.geocities.com/capecanaveral/lab/1029

Several members of **The Tsunami Society** have helped develop a web site for the **Pacific Tsunami Museum** in Hilo, Hawaii. The web site has the following URL:

http://planet-hawaii.com/TSUNAMI

Any other **Tsunami Society** member who is publishing tsunami information on a web site may wish to inform the Editor so that it may be included in future tsunami web site directories.

THE WAVE FORMS AND DIRECTIVITY OF A TSUNAMI GENERATED BY AN EARTHQUAKE AND A LANDSLIDE.

S. I. IWASAKI
National Research Institute for Earth Science and Disaster Prevention,
3-1 Tennodai Tsukuba Ibaraki 305 JAPAN

ABSTRACT

Using a realistic topography of an ocean, differences in wave forms and directivities of tsunamis generated by earthquakes and landslides are investigated through numerical simulations. The ocean is composed of a shelf, shelf slope and bottom regions. Tsunami sources are located on the shelf slope and the bottom region. The length of the tsunami source is 100 km and the width is 50 km. For the earthquake, uniform vertical deformation of 1 m is assumed to jerk instantaneously. For the landslide, solid slab with 50 m thickness is assumed to be moved in off-shore direction with the uniform velocity. The boundary condition on the coastline is solid and elsewhere are open boundaries. The linear long wave simulation model is used.

Tsunamis generated by landslides show strong directivities compared with those generated by earthquakes. But, in the range less than $3\pi/8$ from the direction of the minor axis of tsunami sources, the variation of the directivity coefficients are almost the same regardless of differences in the generation mechanisms, generating regions and the ocean topographies. The ratios of the amplitude of the first crest (trough) to trough (crest) of the waves are roughly unity for the tsunamis generated by earthquakes. But those for the landslides, the ratios are varied from unity to 1/5 depend on the azimuths of the observing points.

1. INTRODUCTION

The two great tsunamis, the Sanriku in 1896 and the Aleutian in 1946, were extraordinary. The tsunami run-up heights observed at coasts were so large in spite of the moderate magnitudes of the earthquakes which generated the tsunamis. The reasons are not fully clear. Slow-earthquake is one of the explanations (Kanamori, 1972). But, landslide is also one of the possibilities. It is well known that landslides generate tsunamis. Recently several large scale landslide traces were found near the Sanriku coast (Honza et al., 1978). And, it was discovered that one of these landslides would have a potential to generate a large tsunami (Iwasaki et al., 1996). Sometimes landslides are triggered by earthquakes. In the Grand Bank earthquake in 1929, a turbidity current was generated and set off tsunami (Heezen and Ewing, 1952). At the time of the Nihonkai-Chubu earthquake in 1983 and Hokkaido Nansei-Oki earthquake in 1993, it was reported that the arrivals of the initial wave of these two tsunamis were observed earlier at several coasts than the expected times. These were explained due to the pre-slips or landslides (Shuto et al., 1993 and 1994). In the Flores island tsunamis in 1992 there exist clear pictures of evidence of landslide trace and this landslide affected the tsunami characteristics locally (Imamura et al., 1993). Nakamura and Arai (1996) reported extraordinary fast arrival of the tsunami at the several coasts along the Okhotsk sea at the time of the Hokkaido Toho-Oki earthquake in 1994 and these waves were generated at the other places, apart from the main shock about 200 km. From the seismicity near this region, they concluded that a landslide is the most probable cause of the fast arrivals.

It is quite possible that landslides generate tsunamis or that landslides triggered by earthquakes affect the tsunami characteristics. It is important to know the difference of the characteristics between tsunamis generated by landslides and tectonic movements to prorate that portion of the tsunamis generated by landslides and that by earthquakes. For tsunamis generated by tectonic movements, Kajiura (1970) discussed the energy and directivity of the wave qualitatively considering various source models in an ocean of constant depth. But, for landslides, this type of study has not been done. In this paper, using the numerical simulation methods, the differences of the directivity and wave forms of tsunamis generated by landslides and tectonic movements are investigated in an realistic ocean model.

2. The MODEL

The schematic view of the model is shown in Fig.1. The Cartesian co-ordinate system

is used with the origin at the center of the coast. The left figure is a plan view of the model and the right is the vertical profile of the ocean. The depth and the length of the continental shelf is 200 m and 100 km, respectively. The slope of the shelf slope is 1/30 and the length is 120 km. The depth of the ocean bottom is 4200 m and the length is 230 km. Tsunami source is located on the shelf slope and the bottom region. The area of tsunami source is 100 km long and 50 km wide. For the earthquake, it is assumed that uniform vertical deformation of 1 m jerked instantaneously. For the landslide, a rectangular slab with thickness 50 m is slid down in the off-shore direction (y-direction) with the uniform velocity. The duration of the landslide is 4000 sec. Three cases of landslide simulations are made by changing the uniform sliding velocity as 5 m/s, 10 m/s and 20 m/s.

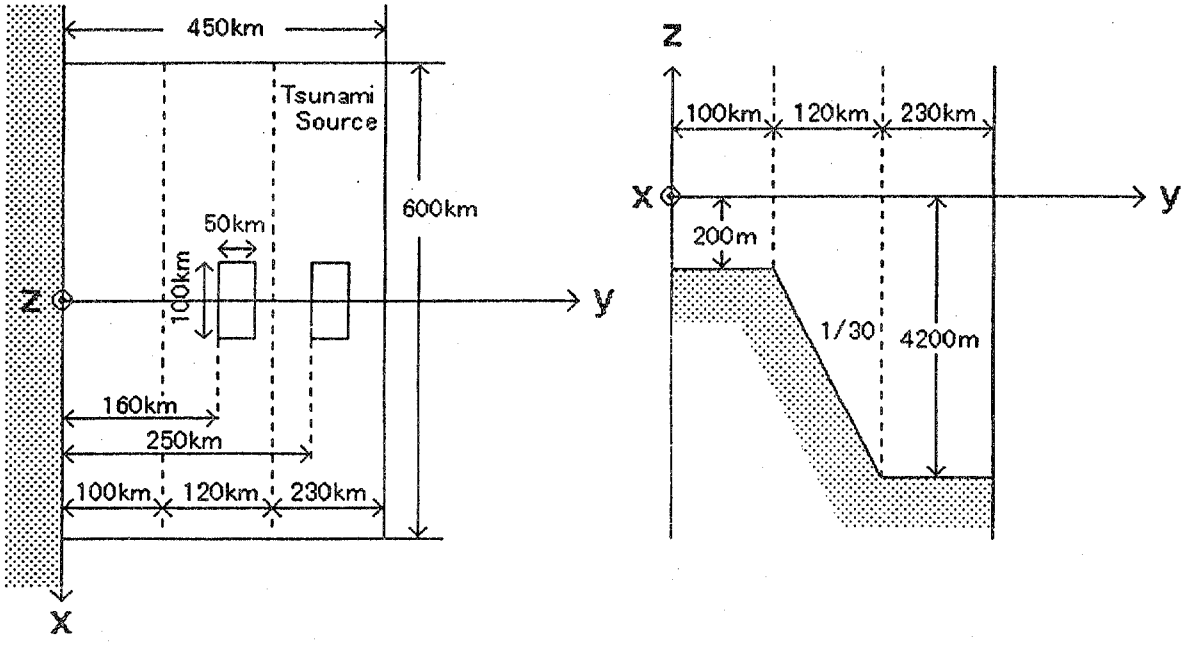

Fig.1 A schematic view of the model.

3. NUMERICAL SIMULATIONS

Under the linear long wave approximation, the basic equations are

$$\frac{\delta \eta}{\delta t} + \frac{\delta M}{\delta x} + \frac{\delta N}{\delta y} = 0, \qquad (1)$$

$$\frac{\delta M}{\delta t} + gd\frac{\delta \eta}{\delta x} = 0, \qquad (2)$$

$$\frac{\delta N}{\delta t} + gd\frac{\delta \eta}{\delta y} = 0, \qquad (3)$$

Where

η **: surface water level,**

M,N: discharge fluxes in x, y directions,

d: water depth and

g: gravity constant.

Since, the ocean bottom deformation is assumed to be an instantaneous jerk, it is converted to the water surface maintaining its shape as the initial condition of the simulation for the tsunami generated by the tectonic movements. For the landslide, the distinguishing point is the source movement. The generating mass moves horizontally and generates successive tsunamis. According to Iwasaki et al. (1996) , the procedure is as follows. The initial wave form of the tsunami due to the landslide is calculated by an analytical method. Then, the initial wave form is transferred to numerical simulation program as the initial condition. The wave form of the next time step produced by the continuing landslide is again calculated analytically. The results of the second step are added to the numerical simulation results of the former step. The routine continues to the end of the movement of the landslide.

As an analytical solution, Kajiura (1963) presented a time dependent Green's function in an ocean of constant depth under the long wave approximation. Using this, the tsunami wave form due to the landslide is given by

$$\eta_A = \frac{V_h}{\pi}\Delta t\{\tanh^{-1}\left(\frac{\sin(\frac{\zeta_0}{2d}\pi)}{\cosh(\frac{x-d}{2d}\pi)}\right) - \tanh^{-1}\left(\frac{\sin(\frac{\zeta_0}{2d}\pi)}{\cosh(\frac{x+d}{2d}\pi)}\right)\}. \qquad (4)$$

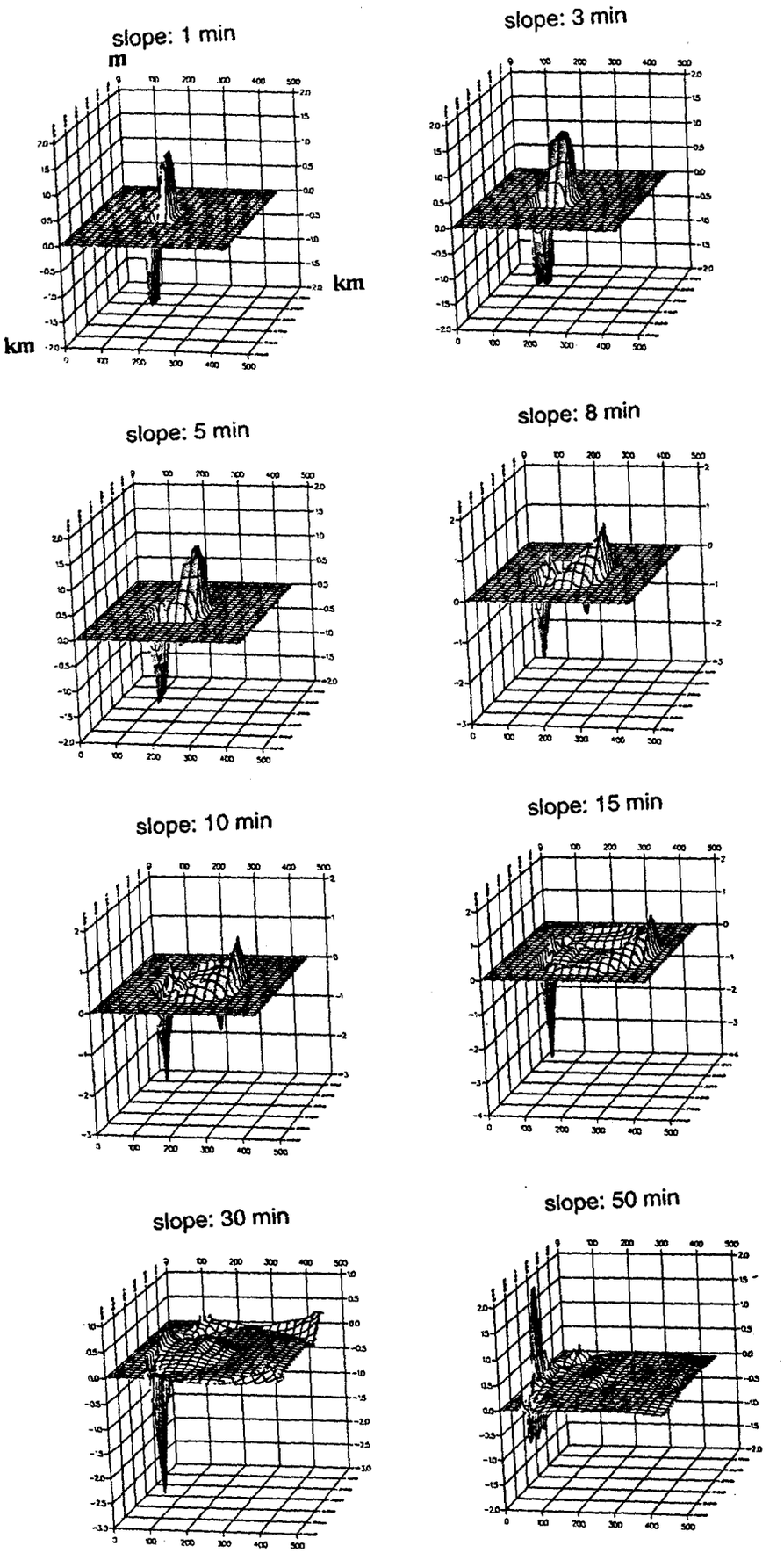

Fig.2 Perspective views of tsunami generated by the landslide. Landslide location is on the shelf slope and the horizontal sliding velocity is 10 m/s.

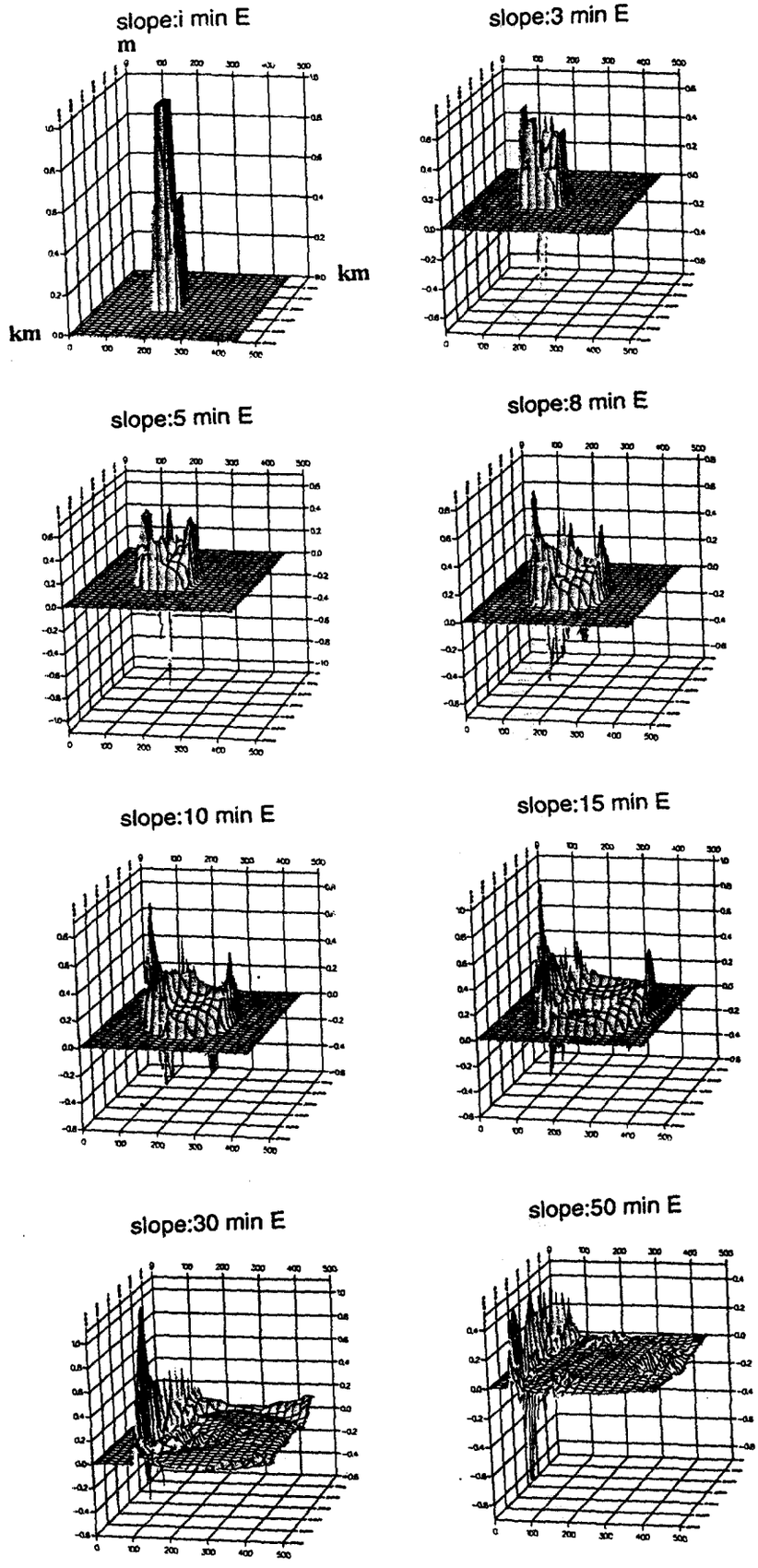

Fig.3 Perspective views of tsunami generated by the earthquake. The uniform vertical deformation of 1 m is jerked instantaneously on the shelf slope.

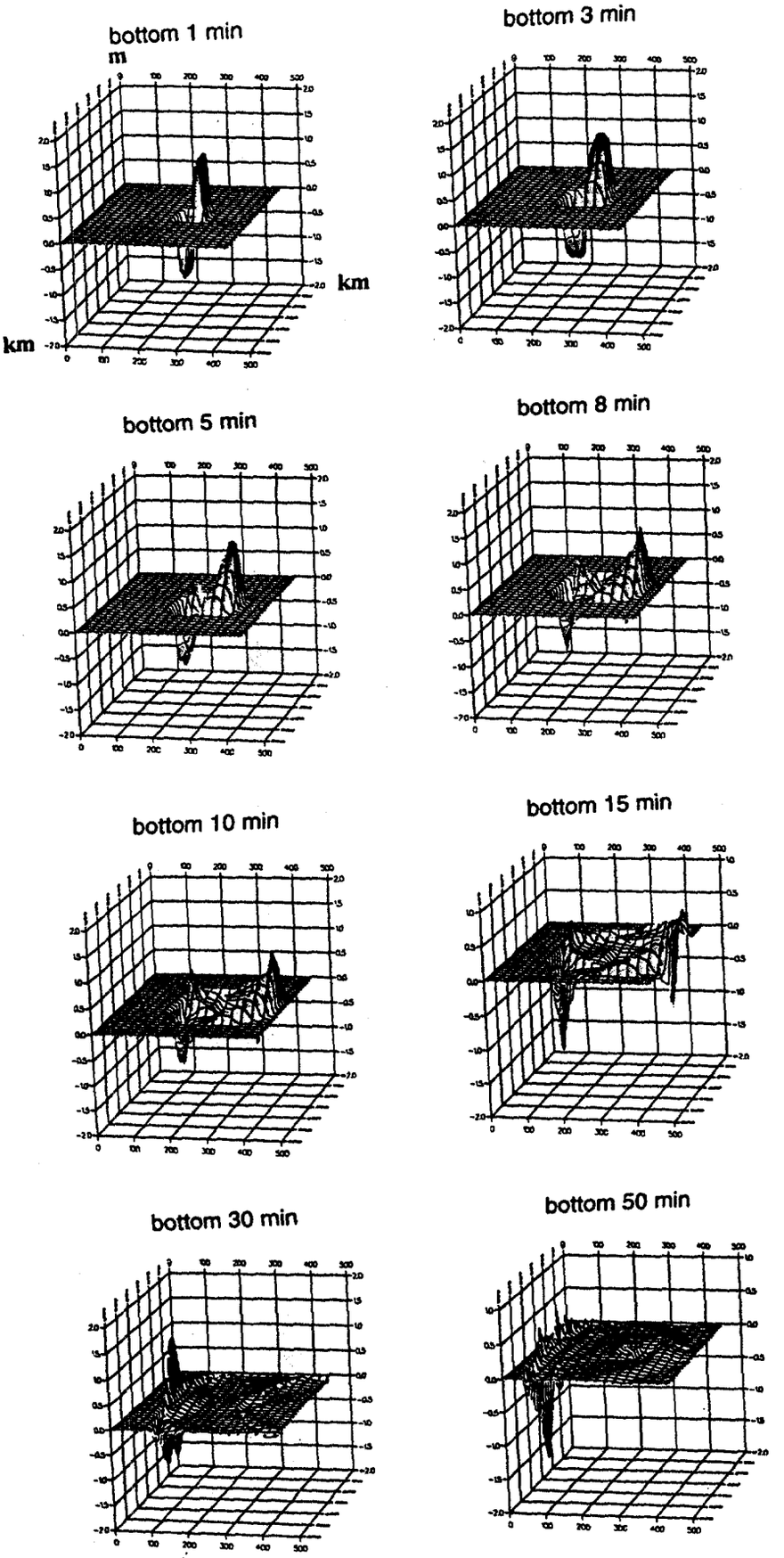

Fig.4 A same figure as Fig.2, but, the landslide location is on the bottom.

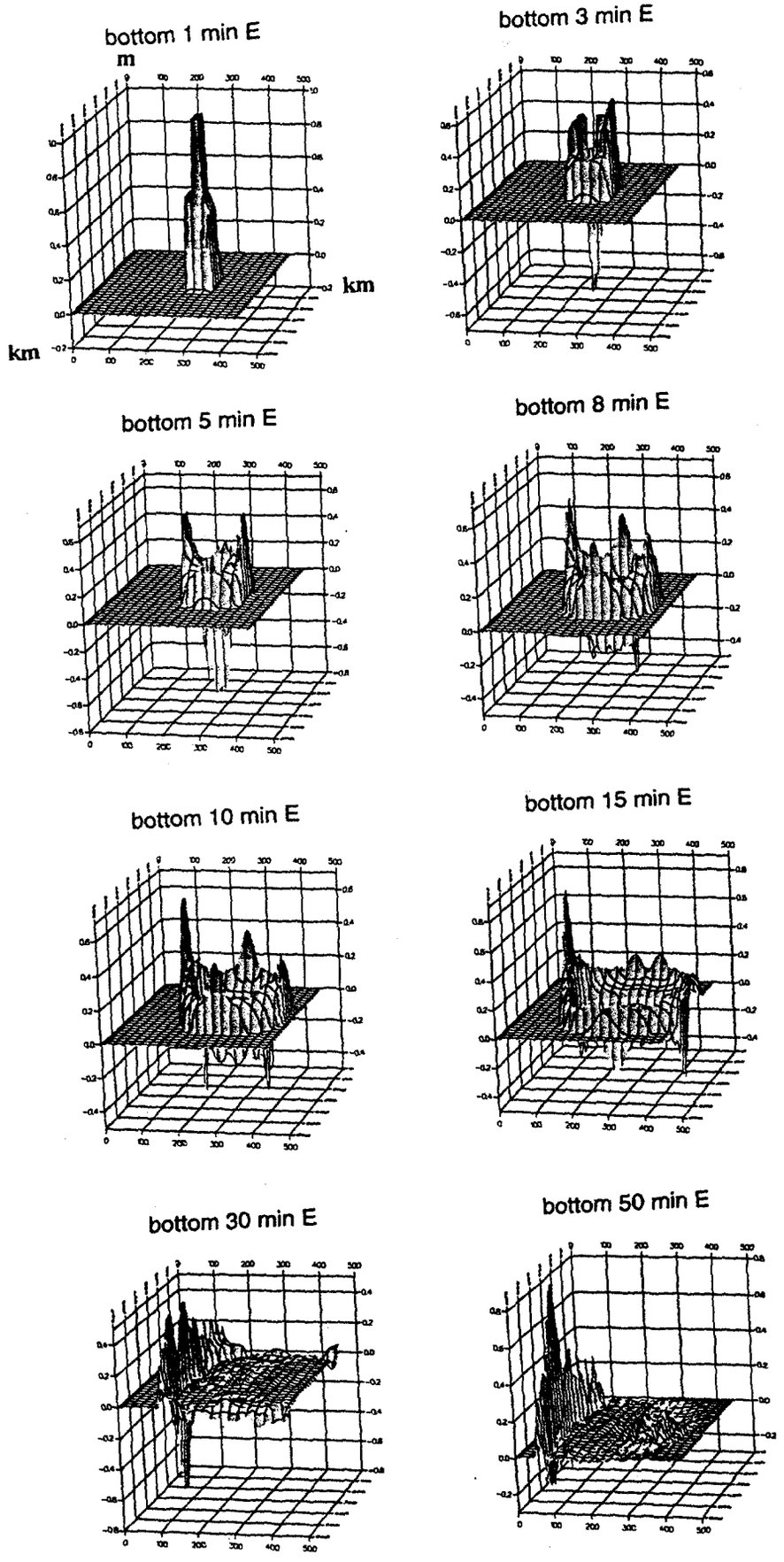

Fig.5 A same figure as Fig.3, but, the earthquake location is on the bottom.

Tsunami is generated at the front and rear side of the landslide. The above solution is valid only for an constant depth ocean. However the solution decays very rapidly with the distance. So, this solution was used as the initial and successive tsunami wave forms due to landslide even in the sloping region as the water depth is locally constant.

4. THE RESULTS

Fig. 2, 3, 4 and 5 are perspective views of tsunamis generated by landslides for the case of the sliding velocity being 10 m/s and earthquake. The vertical scale is in m and the horizontal scale is in km. The time measured from the onset of landslide and earthquake are shown in the upper side of each figure. Here, SLOPE means tsunami source is located on the shelf slope, BOTTOM means the source located on the bottom region and E means that this is the tsunami generated by an earthquake.

Differences of wave forms due to the generating region locations are not clear from the perspective views. For the earthquake, up to 8 min. the directivity is not changed drastically for both cases. Rather small peaks exist in the directions of the major and minor axis directions of tsunami sources. After 10 minutes from the onset of the earthquakes, on-shore side wave height enlarges because the water depth became shallow. For the landslides, both for the tsunami source located on the shelf slope and the bottom, the difference of wave heights shows strong directivity even at 3 minutes from the onset of landslides. Due to the successive tsunami generations, small peaks and troughs are shown in the region after the first wave propagates to outside.

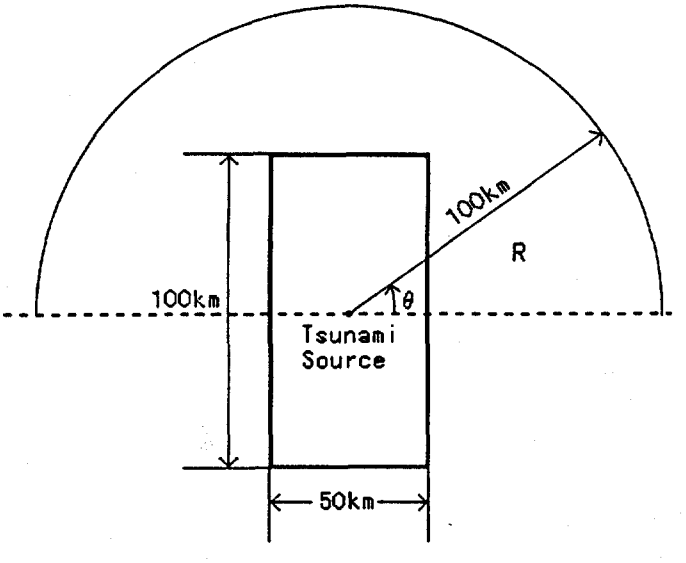

Fig.6 Observing points arrangement.

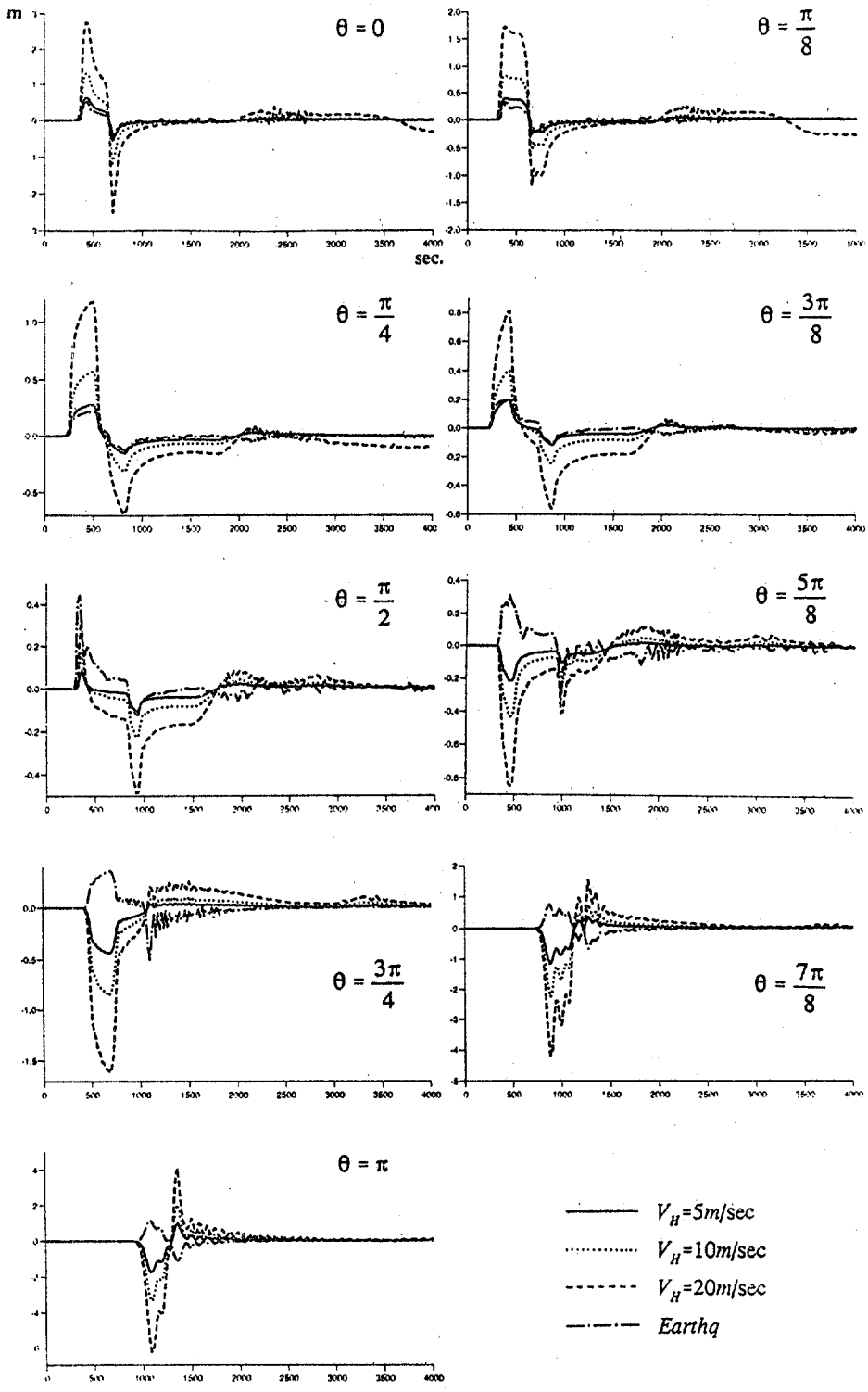

Fig.7 Tsunami wave forms as a function of the time. Tsunami sources are located on the shelf slope.

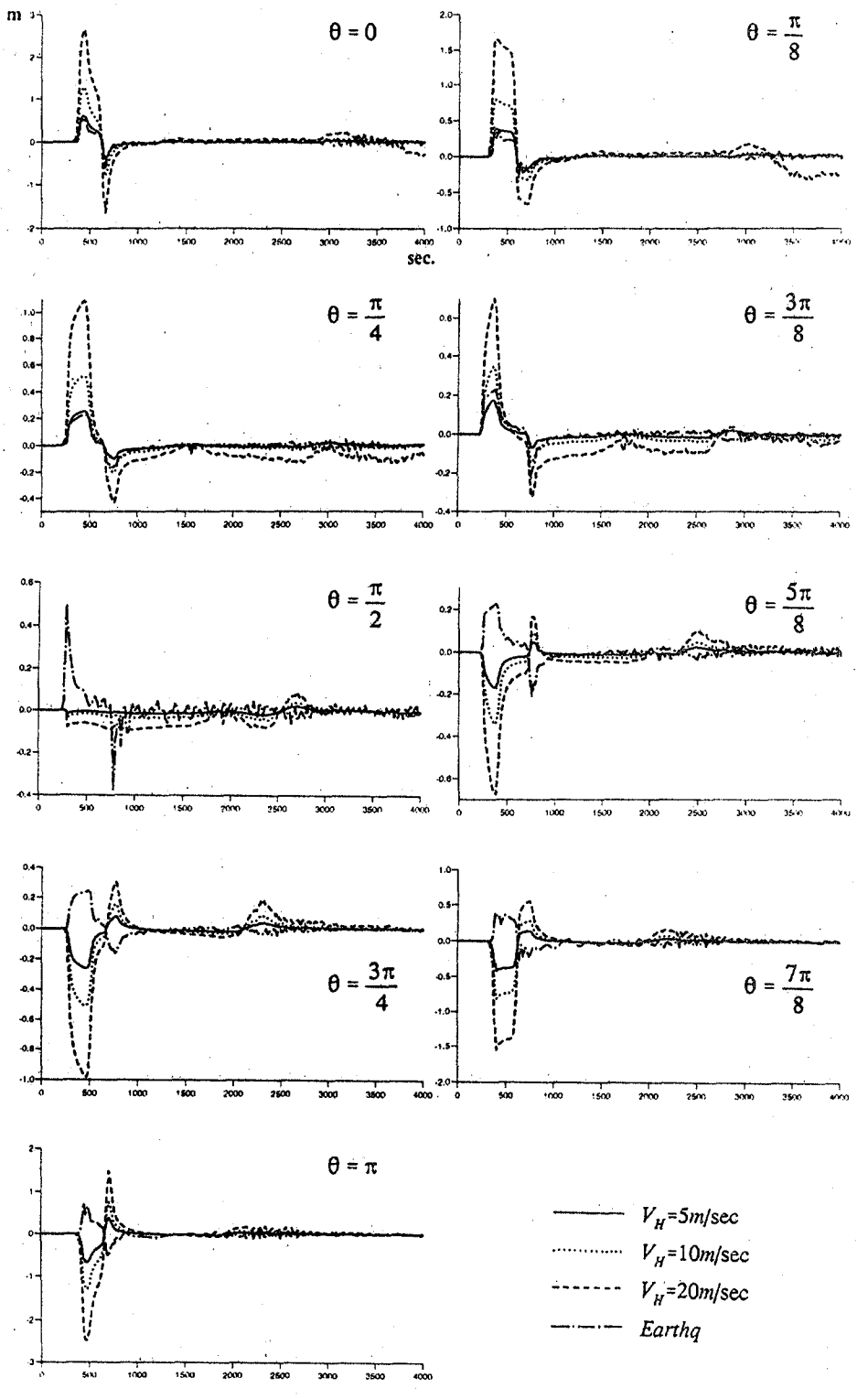

Fig.8 A same figure as Fig.7, but, tsunami sources are located on the bottom.

Several observing points were picked up to see the time dependence of wave forms. Fig.6 shows a observing points arrangement. The points were located at the distance of 100 km from the center of the tsunami source. The azimuths were measured in a counter clockwise manner and off-shore direction of the minor axis of tsunami source is selected as θ=0.

Fig.7 and 8 shows tsunami wave forms as a function of the time. The vertical scale is in m and the horizontal scale is in second.For most of the observing points, the waves are composed of a single crest and trough. The wave forms due to earthquake and landslide are quite similar, in particular, at θ=0 and $\theta = \pi/2$. But, the sign is converted for $\theta = \pi/2$. The duration of the first elevated (or, depressed) portion in each waves is roughly correspond to the length of the tsunami source projected in the direction of the observing point. Significant differences of wave forms due to the differences of generation mechanisms are restricted less than $\pi/8$ from the directions of the major axis of tsunami source. The ratios of the first crest (trough) to trough (crest) are roughly unity in case of earthquakes but the ratios vary from unity to 1/5 in case of landslides. The differences due to the location of the tsunami source are significant at $\theta = 3\pi/4$, $\theta = 7\pi/8$ and $\theta = \pi/2$, these are the direction of the rear side of the landslides movements. This is because the differences of superpositions of successive wave trains of a tsunami. That is, in the direction of the front side, the position of the first wave crest and that of the second one are more closer than those in the direction of the rear side and this tendency is emphasized in case of the tsunami source is on the shelf slope.

Directivity coefficients are calculated for the earthquake and three cases of landslides. The total flux of gravity wave energy E_f for the unit width, transmitted in the peculiar direction can be computed approximately by following the formula, because the wave can be considered as a progressive after leaving the tsunami source.

$$E_f = \rho g \int_0^\infty \eta^2 c dt, \qquad (5)$$

where

ρ denotes the density of the water and c denotes the phase velocity.

The directivity coefficient Q is defined as

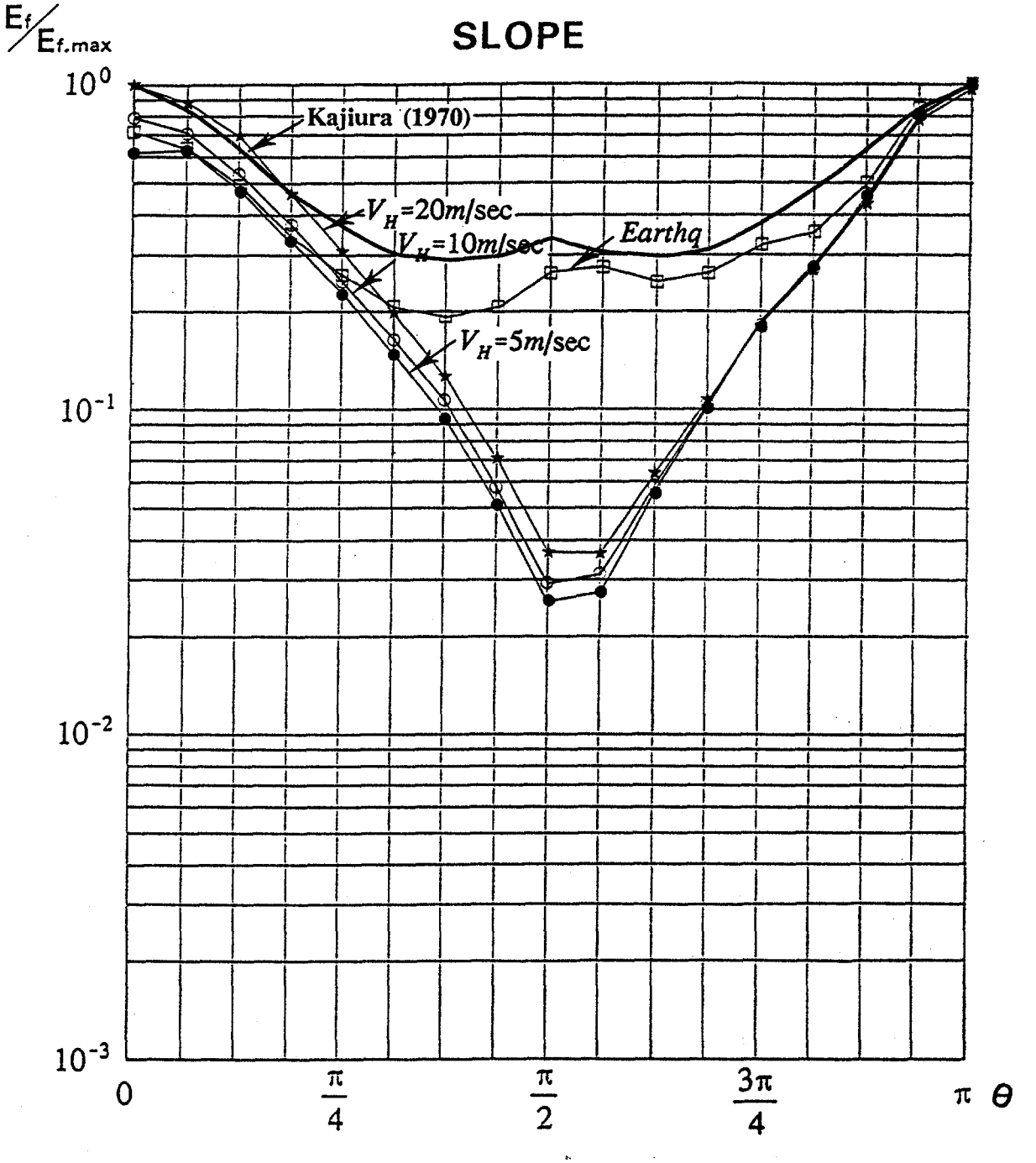

Fig.9 Directivity coefficients as a function of azimuth of the observing point in case of tsunami sources are located on the shelf slope.
Kajiura's (1970) solution is also shown in comparison.

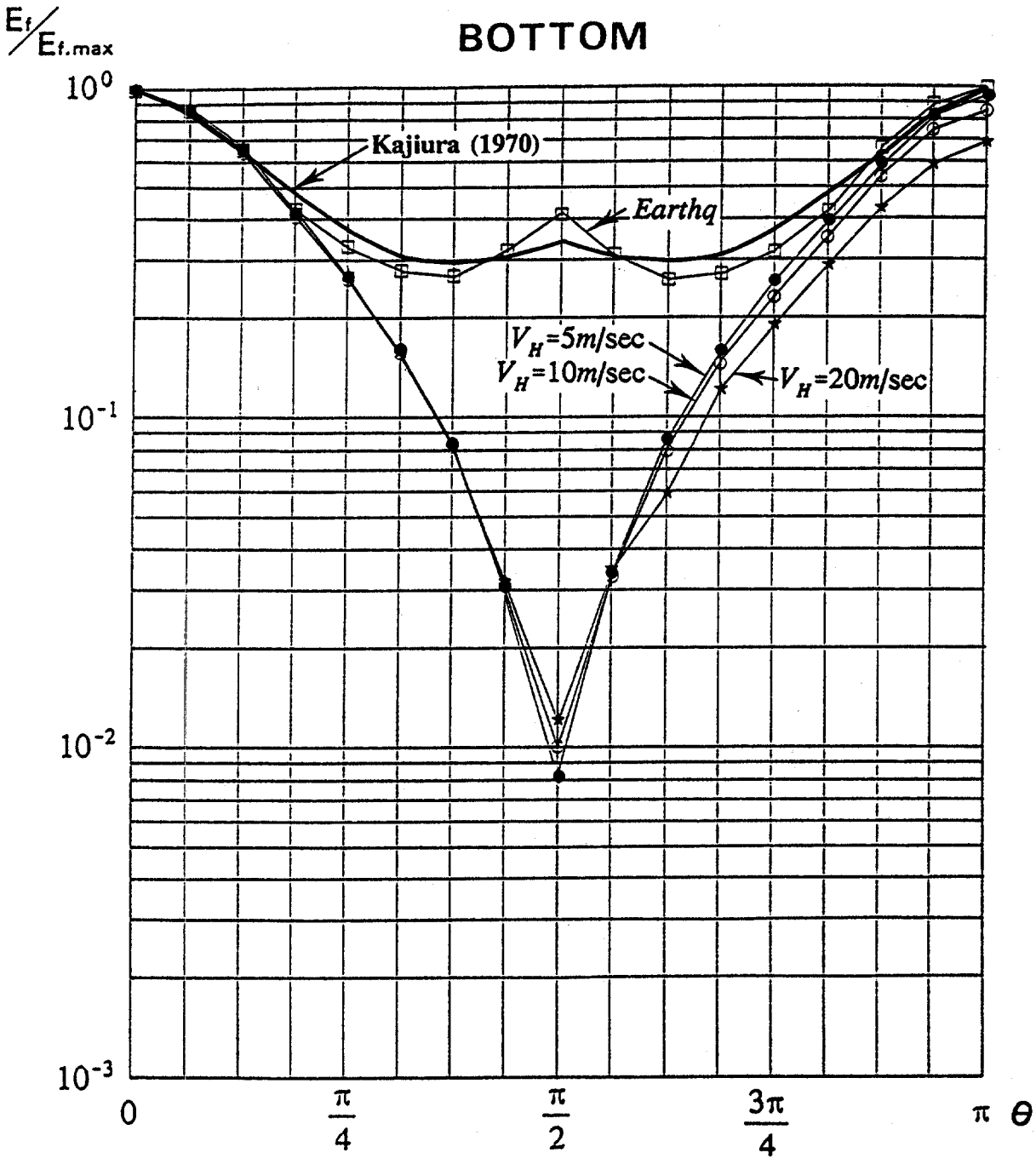

Fig.10 A same figure as Fig.9,but, tsunami sources are located on the bottom.

$$Q = E_f / E_{fmax} . \qquad (6)$$

where, E_{fmax} is the maximum value of E_f for each cases.

Fig.9 and 10 shows the directivity coefficients Q as a function of θ in case of tsunami source located on the shelf slope and the bottom, respectively. In these figures Kajiura's (1970) result is also shown for the comparison. He calculated the directivity coefficients in the range of $0 < \theta < \pi/2$ for the tectonic movement by earthquake in an ocean of constant depth. Since, the ocean in his model was constant depth, his results can be extended in the range of $\pi/2 < \theta < \pi$ assuming the symmetry relative to $\theta = \pi/2$. In his case, the distance of the observing points from the center position of the tsunami source were 200 km whereas it is 100 km in the present study.
The ratios of the maximum value to the minimum value of Q in each cases are calculated and shown in Table.1

locations mechanisms	shelf slope on-shore	shelf slope off-shore	bottom on-shore	bottom off-shore
landslide: V_H=5 m/s	0.0359	0.0256	0.00830	0.00878
landslide: V_H=10 m/s	0.0370	0.0295	0.0100	0.0117
landslide: V_H=20 m/s	0.0366	0.0374	0.0120	0.0174
earthquake	0.278	0.247	0.266	0.262

Table 1. The ratios of the maximum to the minimum values of E_f.

The variation of directivity coefficients are large in case of landslides compared with those in case of earthquakes, in particular, in case of the tsunami source located on the bottom region. For the earthquakes, the variations of Q are significant in the range $0 < \theta < \pi/4$ and $3\pi/4 < \theta < \pi$, while in the range $\pi/4 < \theta < 3\pi/4$, the values are almost constant.

The variations of Q are almost symmetric relative to the direction of the major axis

of tsunami source ($\theta = \pi/2$) for the case of the source located on the bottom region, but, for the case of the source located on the shelf slope, there exist somewhat differences of the variation of Q in the ranges $0 < \theta < \pi/2$ and $\pi/2 < \theta < \pi$. The total energy flux propagating in the on–shore direction is a little bit large compared with that to the off–shore direction. The most significant characteristics is the variations of the directivity coefficient being almost the same from $\theta = 0$ to $\theta = 3\pi/8$ regardless of the differences of the generation mechanisms, the generating regions and the ocean topography. The discrepancy of the variation of the directivity coefficients due to the difference of the generation mechanisms are obvious from $\theta = \pi/4$ for the tsunami source located in the shelf slope and from $\theta = 3\pi/8$ for that in the bottom region.

5. CONCLUDING REMARKS

In the present paper, the differences of wave forms and directivities of tsunamis due to the differences of generation mechanisms and generation regions for a realistic ocean topography are discussed through the numerical simulations. Following conclusions are found.

(1) Differences of generation mechanisms:

- wave forms of tsunamis generated by tectonic movements and landslides are quite similar in the direction of the minor axis of tsunami sources.
- the variations of the directivities coefficient are large for tsunamis generated by landslides compared with those for tectonic movements.

(2) Differences due to the generation regions.

- wave forms are quite similar near the directions of minor axis of tsunami sources, but, the slight differences exist near the major axis of tsunami sources.
- Variations of directivity coefficients are large for tsunamis generated by landslides on the bottom compared with those on the shelf slope. On the contrary, for tsunamis generated by earthquakes, this tendency is reversed.

The most significant characteristics is that the wave forms and the variations of directivity coefficients are almost the same in the range less than $3\pi/8$ from the direction of the minor axis of tsunami sources regardless the differences of generation mechanisms, generation regions and the ocean topographies. It suggests strongly that if the azimuths of the observing points are distributed in a narrow region, it is difficult to know what potion of a tsunami was generated by an earthquake and what portion by landslide.

ACKNOWLEDGEMENT

The simulation program used in the present study was originally developed at the Tohoku University under the TIME (Tsunami Inundation Model Exchange) project and modified by the author. Thanks are also extended to Ms. S.Kashimura for assistances in the various phases of this study.

REFERENCES

Heezen, B.C. and M. Ewing, 1952, Turbidity Currents and Submarine Slumps, and the 1929 Grand Bank Earthquake, American Journal of Science, 250, 849–873.

Honza, E., 1978, Geological map of Japan trench, 1/1 million, Marine Geol. Map. Ser. 11, Geol. Surv. Japan.

Imamura, F., H. Matsutomi, Y. Tsuji, M. Matsuyama, Y. Kawata and T. Takahashi, 1993, Field Survey of the 1992 Indonesia Flores Tsunami and its analysis, Proc. Coastal Engineering, JSCE, 40, 181–185 (J).

Iwasaki, S. I., A. S. Furumoto and E. Honza, 1996, Can a Submarine Landslide be Considered as a Tsunami Source?, Science of Tsunami Hazards, 14, In printing.

Kajiura, K., 1963, The leading Wave of a Tsunami, Bull. of the Earthq. Res. Inst., 41, 535–571.

Kajiura, K., 1970, Tsunami Source, Energy and the Directivity of Wave Radiation, Bull. of the Earthq. Res. Inst., 48, 835–869.

Kanamori, H., 1972, Mechanism of Tsunami Earthquakes, Phys. Earth Planet. Interiors, 6, 346–359.

Nakamura, K. and K. Arai, 1996, A Small Tsunami Observed along the Coast of the Okhotsk Sea Accompanied with the 1994 Hokkaido Toho–Oki Earthquake, ZISIN, 48, 451–461 (J).

Shuto, N., K. Chida and F. Imamura, 1993, Generation Mechanism of the 1983 Nihonkai–Chubu Earthquake Tsunami, Proc. IUGG/IOC ITS'93, Wakayama, 9–21.

Shuto, N., H. Matsutomi and M. Unohana, 1994, Characteristics of the Hokkaido Nansei-Oki Earthquake Tsunami and the Problems for the Further Study, Proc. Coastal Engineering, JSCE, 41, 236-240 (J)

MODELING THE 1994 SKAGWAY TSUNAMI

Charles L. Mader
Mader Consulting Co.
Honolulu, Hawaii 96825-2860 U.S.A.

ABSTRACT

On November 3, 1994, a Tsunami wave with a period of 3 minutes and maximum height of 25 to 30 feet occurred at Skagway, Alaska in the Taiya Inlet. The wave was observed traveling along the PARN dock from the South or deep end of Taiya Inlet.

The tsunami has been proposed to have been caused by a landslide at the dock or in the inlet. Possible landslides have been numerically modeled using the SWAN code to evaluate the various proposed sources.

The dock landslide generated a tsunami wave with much shorter wave periods than observed (less than a third). The direction of the wave was 90 degrees different than observed. Since the dimensions of the slide used in the model were about as large as possible from the surveys, the dock landslide alone could not have generated the observed tsunami wave.

The sea floor elevations before and after the event indicate that a considerable area of the sea floor was lower for about 5000 feet down the inlet and then much of the sea floor was higher further down the inlet. The complicated bottom topography changes that occurred were described in the numerical model using a 3 slide region model. The landslides generated a tsunami wave with about the wave amplitude and period observed. The direction of the wave was the same as observed along the dock.

INTRODUCTION

On November 3, 1994, at about 7:10 p.m., a Tsunami wave with a period of about 3 minutes and maximum height of 25 to 30 feet occurred in the Taiya Inlet at Skagway, Alaska as reported by Lander(1). The event occurred at the time of a low tide of 4 feet below lower low level. The tidal range at Skagway is about 25 feet. The wave was observed traveling along the Pacific and Arctic Railway and Navigation Company (PARN) dock from the South or deep end of Taiya Inlet. The sea floor elevations before and after the event indicate that a considerable area of the sea floor was lower for about 5000 feet down the inlet and then much of the sea floor was higher further down the inlet as described by Campbell in references 2 and 3. The sea floor elevation changes had a volume of 20 to 25 million cubic yards.

Kulikov, Rabinovich, Thomson and Bornhold (4) proposed that the tsunami was caused by the collapse of the PARN dock. Their slide involved sediment of 10 to 20 meters thick and extended 125 to 200 meters offshore. Lander(1) estimated the dock slide to have been 600 feet wide, 50 to 60 feet thick, and 4,500 feet long with a total volume of 1 to 3 million cubic yards.

From eye witness reports, Bruce Campbell (3) has reconstructed the chronology of events.

Time	Event
-2 min	Wind Stopped
0-2 sec	Dock Construction Sheet Piles Rattled, Crane Moved
2-3 sec	Dock and Sheet Piles Started to Slide Seaward
3-4 sec	Ground Fell out from Under P. Wallin
4 sec	P. Wallin was hit with falling wood pile
4-5 sec	Observers saw Incoming Wall of Water from South End of Dock
4-5 sec	Observers saw Wave with South dock decking and Gangway
4-5 sec	Wall of Water Moving Along Dock Seen Before Sheet Piles Disappeared
6 sec	Blue Work Barge was Visible Above Top of Dock
17-19 sec	Ferry Terminal Lights Disappeared
18 sec	Loud Crash and Boom from Ferry Terminal
120+ sec	Workman Returned to Crane on North End of Dock
120+ sec	Section of South Dock and Gangway was at End of North Dock

The NOAA tide gauge was situated midway along the ore dock on the west side of the harbor. The tsunami recorded by this gauge on November 3, 1994 had a period of approximately 3 minutes, a maximum recorded amplitude of about 3 feet and lasted for about 30 minutes. The Skagway tide gauge was a damped nitrogen bubbler analog gauge which gives a nonlinear response at short periods. Thus the recorded wave heights are considerably smaller than those of the actual tsunami. To determine the tsunami wave heights, Irwin and Nottingham in reference 3 determined the water tower-generated tide gauge trace that would duplicate the tsunami tide gauge record. The details of the time and wave heights that matched the Skagway tidal chart tsunami are shown in Figure 1.

The tsunami wave had an initial amplitude of 12 feet and period of 60 seconds followed by 3 waves with amplitudes of 6 to 9 feet and period of 180 seconds.

Raichlen, Lee, Petroff and Watts (5) also calibrated the Skagway tide gauge. For excitation periods greater than 1000 seconds, they found that the gauge gave the wave amplitude. For periods of 3 minutes the gauge gave amplitudes that were 40 to 75 percent of the actual wave amplitude. For periods of 20 to 30 seconds the gauge gave amplitudes that were 5 to 24 percent of the actual wave amplitude.

MODELING

The generation and propagation of the tsunami wave of November 3, 1994 in the Taiya Inlet was modeled using a 23 by 23 meter grid of the topography. The modeling was performed using the *SWAN* non-linear shallow water code which includes Coriolis and frictional effects. The *SWAN* code is described in reference 6. Various applications of the SWAN code are described in references 7 thru 28. The calculations were performed on a 166 Mhz Pentium personal computer. A 3 by 6 second land topography was generated from the Rocky Mountain Communication's CD-ROM compilation of the Defense Mapping Agency (DMA) 1 x 1 degree blocks of 3 arc second elevation data. The 23 by 23 meter land topography was generated by interpolation. The sea floor topography before the event was generated by T. Gere of PN&D and Z. Kowalik of the University of Alaska. The grid was 160 by 400 cells and the time step was 0.15 second.

DOCKSLIDE MODEL

About 750 feet of the dock was destroyed and the slope supporting the dock slid into deep water. The sea floor elevation below the dock area was about 100 feet lower after the event. To model the dock landslide an extreme case was considered. A 740 feet along the dock by 1500 feet wide region was lowered by 100 feet and then the seaward 740 feet by 1500 feet region was raised by 100 feet. The dock slide geometry is shown in Figure 2.

The calculated wave profile at the south end of the PARN dock (cell (143,227) at 28 meter depth) and the wave profile at the tide gauge (cell (140,245) at 13 meter depth) are shown in Figure 4.

INLET LANDSLIDE MODEL

The landslide model studied was that described by Bruce Campbell in references 2 and 3 from the change in the sea floor topography that occurred before and after the tsunami. The Campbell model consists of three slide regions separated by ridges. The west slide region was approximately 1000 feet wide, 4000 feet long and a volume of 11.35 million cubic yards. The middle slide region was 500 feet wide, 3600 feet long and had a volume of 5.1 million cubic yards. The east slide region was 400 feet wide, 4800 feet long and had a volume of 5 million cubic yards.

The material from the three slides moved down into the deep part of the inlet occupying an area 3000 feet wide by 5800 feet long with a volume of 21.5 million cubic yards.

The profiles of the slide depths showed that the upper regions of each slide was thicker than the rest of the slide. The slide regions were described by a thicker upper region followed by a less thick lower region.

The Campbell 3 slide model is shown in Figure 3 and was described numerically as follows:

West Slide - upper region -1056 by 1056 by 137.8 feet deep.
West Slide - lower region -1056 wide by 2942 long by 49.2 feet deep.
West Slide - Total Volume of 11.35 million cubic yards.

Middle Slide - upper region -528 wide by 1207 long by 118.8 feet deep.
Middle Slide - lower region -528 wide by 2414 long by 49.2 feet deep
Middle Slide - Total volume of 5.11 million cubic yards.

East Slide - upper region -377 wide by 1131 long by 98.4 feet deep.
East Slide - lower region -377 wide by 3696 long by 65.6 feet deep
East Slide - Total Volume of 4.94 million cubic yards.

Slide Debris - 3017 wide by 5809 long by 32.8 feet thick.
Slide Debris - Total Volume of 21.3 million cubic yards.

The calculated wave profile at the south end of the PARN dock (cell (143,227) at 28 meter depth) and the wave profile at the tide gauge (cell (140,245) at 13 meter depth) are shown in Figure 5 for the landslide displacement occurring instantaneously.

The time for the landslide to occur was varied from 0 to 3 minutes. The calculated wave period difference for the landslide and dockslide was insensitive to the time for the landslide to occur and also to whether the upper half of the landslide occurred as 3 slides or as a single slide.

The tide gauge duration and profile was best reproduced by the 2 minute duration slide (about 60 miles/hour). The calculated and calibrated tide gauge profiles are compared in Figure 6. The initial 50 second wave was not reproduced by any of the models. The initial part of the tide gauge record will require further study. The observed and calculated 30 minute duration of the tide gauge record is a result of the resonance for 3 minute waves in the harbor where the tide gauge is located. The waves are decayed outside the harbor after 10 minutes. A similar harbor resonance was described in reference 5.

CONCLUSIONS

The dock landslide generated a tsunami wave with much shorter wave periods than observed (less than a third). The direction of the wave was 90 degrees different than observed. Since the dimensions of the slide used in the model were about as large as possible from the surveys, the dock landslide could not have generated the observed tsunami wave.

The complicated bottom topography changes that occurred were described in the numerical model using a 3 slide region model. The landslides generated a tsunami wave with about the wave amplitude and period observed. The direction of the wave was the same as observed along the dock.

REFERENCES

1. James F. Lander, "Tsunamis Affecting Alaska 1737-1996" NGDC Key to Geophysical Research Documentation No 31 (1996).
2. Bruce Campbell, "Report of a Sea floor Instability at Skagway, Alaska - November 3, 1994" Campbell and Associates Report of January 16, 1995.
3. Bruce Campbell, "Skagway Seafloor Instability Re-Analysis and Update" Campbell and Associates Report of January 28, 1997.
4. E. A. Kulikov, A. B. Rabinovich, R. E. Thomson and B. D. Bornhold, "The Landslide Tsunami of November 3, 1994, Skagway Harbor, Alaska" *Journal of Geophysical Research* **101**, 6609-6615 (1996).
5. Fredric Raichlen, Jiin Jen Lee, Catherine Petroff, and Philip Watt, "The Generation of Waves by a Landslide: Skagway, Alaska – A Case Study," Proceedings of 25th International Conference on Coastal Engineering, 1996.
6. Charles L. Mader, **Numerical Modeling of Water Waves,** University of California Press, Berkeley, California (1988).
7. Charles L. Mader, "Asteroid Tsunami Inundation of Hawaii," *Science of Tsunami Hazards* **14**, 18 (1996).
8. Anthony T. Jones and Charles L. Mader, "Modeling of Tsunami Propagation Directed at Wave Erosion on Southeastern Australia Coast 105,000 Years Ago," *Science of Tsunami Hazards* **13**, 45 (1995).
9. Carl Johnson and Charles L. Mader, "Modeling the 105 Ka Landslide Lanai Tsunami," *Science of Tsunami Hazards* **12**, 3 (1994).
10. Charles L. Mader, Dennis W. Moore and George F. Carrier, "Numerical Tsunami Propagation Study - III," *Science of Tsunami Hazards* **11** , 93 (1993).
11. Charles L. Mader, Dennis W. Moore and George F. Carrier, "Numerical Tsunami Source Study - II," *Science of Tsunami Hazards* **11**, 81 (1993).
12. Charles L. Mader, "Modeling the 1992 Nicaragua Tsunami," *Science of Tsunami Hazards* **11**, 107 (1993).
13. Charles L. Mader, George D. Curtis and George Nabeshima, "Modeling Tsunami Flooding of Hilo, Hawaii," *Recent Advances in Marine Science and Technology, 92* 79-86 PACON International (1993).
14. Charles L. Mader, "Numerical Modeling of Tsunami Waves," *Scientific Computing and Automation* **June**, 19-23 (1993).
15. Charles L. Mader and George Curtis, "Modeling Hilo, Hawaii Tsunami Inundation," *Science of Tsunami Hazards* **9**, 85 (1991).
16. Charles L. Mader, "A Tsunami Flooding Parameter Study," Proceedings of International Symposium on Geophysical Hazards in Developing Countries and their Environmental Impacts, (1991).
17. Charles L. Mader, "Numerical Tsunami Flooding Study - I," *Science of Tsunami Hazards* **8**, 67 (1990).
18. Charles L. Mader, "Numerical and Hydraulic Modeling of Flooding," 2nd UNJR Tsunami Workshop Proceedings, (1990).
19. F. I. Gonzalez, C. L. Mader, M. C. Eble and E. N. Bernard, "The 1987-88 Alaskan Bight Tsunamis: Deep Ocean Data and Model Comparisons," *International Journal of*

Natural Hazards **4**, 119-140 (1991).

20. Charles L. Mader, "Modeling Tsunami Flooding," Proceedings of the Pacific Congress on Marine Science and Technology, PACON 90, July 16-20 (1990).
21. F. I. Gonzalez, E. N. Bernard, M. C. Eble and Charles L. Mader, "Three Recent Alaskan Tsunamis: Deep Ocean Measurements and Model Results," Proceedings of International Tsunami Symposium (1989).
22. "Oahu Intraisland Ferry System - Draft Environmental Impact Statement," State Department of Transportation, Harbors Division (1988).
23. C. L. Mader, M. Vitousek, and S. Lukas, "Numerical Modeling of Atoll Reef Harbors," **Natural and Man-Made Hazards**, M. I. El-Sabh and T. S. Murty, editors, D. Reidel Publishing Co., Dordrecht, Netherlands (1987).
24. Charles L. Mader, "Three-Dimensional Modeling of Tsunamis," Proceedings of the 1985 International Tsunami Symposium, Victoria, Canada, August (1985).
25. Charles L. Mader and Sharon Lukas, "Numerical Modeling of Waianae Harbor," Hawaiian Ocean Experiment, Hawaii Institute of Geophysics Special Publication, pp. 315-324 (1985).
26. Charles L. Mader, "A Landslide Model for the 1975 Hawaii Tsunami," *Science of Tsunami Hazards* **2**, 71 (1984).
27. C. L. Mader, R. E. Tangora, and B. D. Nichols, "A Model of the 1975 Hawaii Tsunami," *Natural Science of Hazards*, C-1, October (1982).
28. Charles L. Mader, "Numerical Simulation of Tsunamis," *Journal of Physical Oceanography* **4**, 74 (1974).

Figure 1. The tsunami wave profile that reproduced the tide gauge record shown.

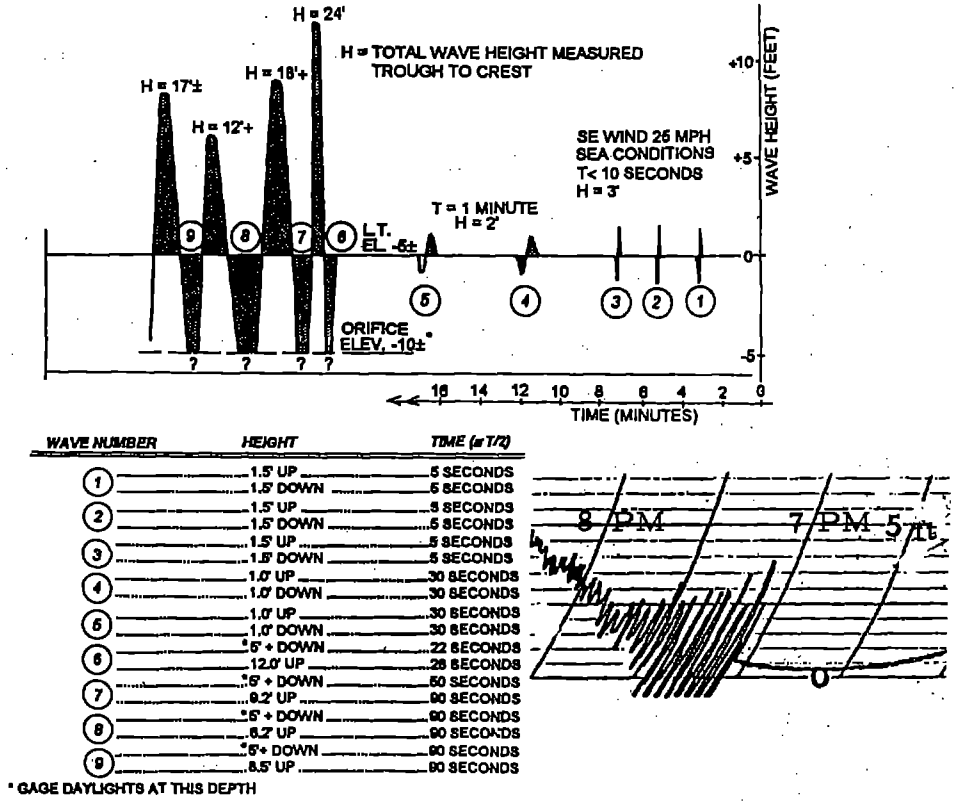

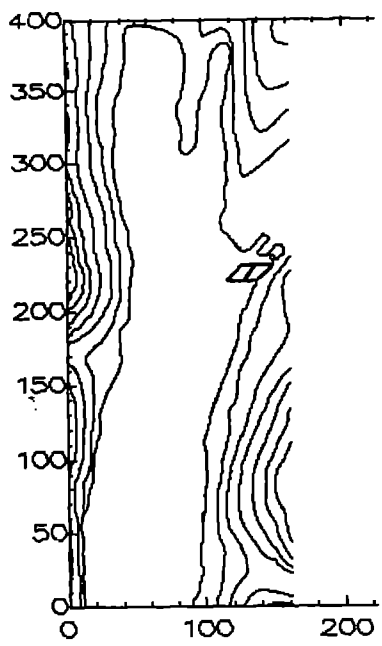

Figure 2.

The Dockslide model. The dockslide had dimensions of 450 by 225 by -30 meter drop near the shoreline and 450 by 225 by 30 meters uplift seaward. The axis scale is in mesh units of 23 meters.

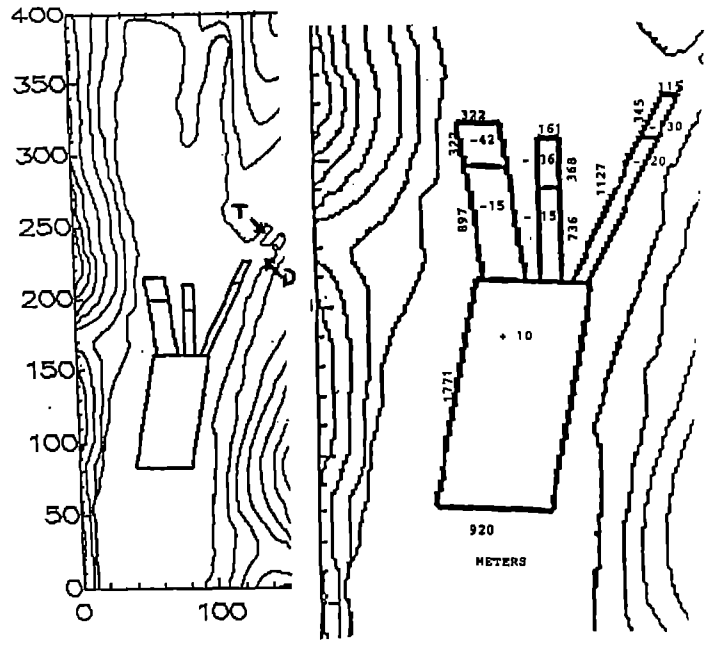

Figure 3. The Campbell 3-slide Landslide model. The dimensions are in meters. The axis scale is in mesh units of 23 meters. The locations of the tide gauge (T) (cell 140,245 - Location 6) and the south end of the PARN dock (D) (cell 143,227 - Location 5) are shown.

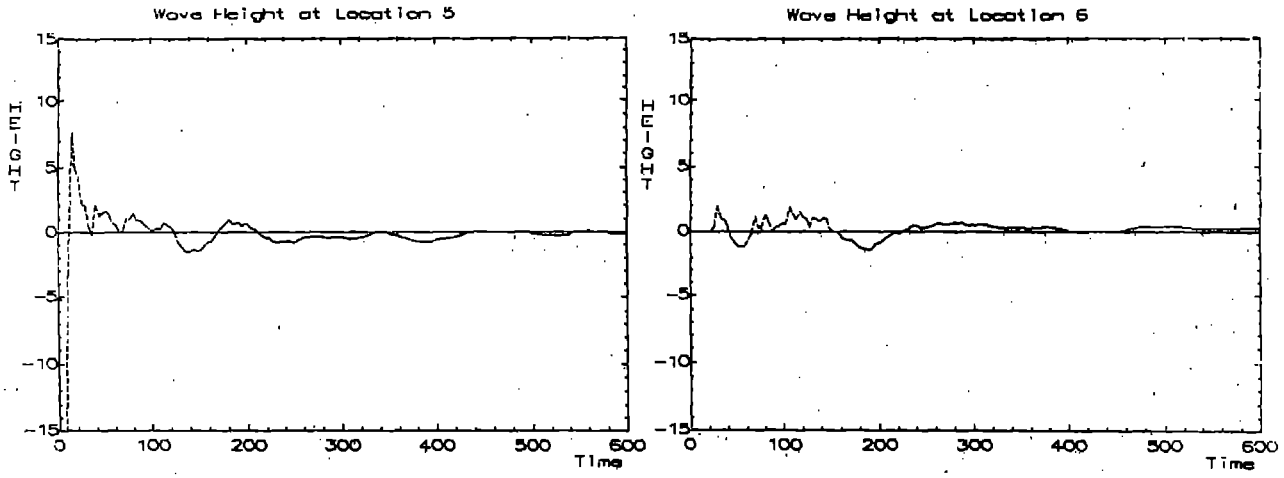

Figure 4. The wave profiles at the south end of the PARN dock (Location 5) and at the tide gauge (Location 6) are shown for the Dockslide model. The vertical axis is height in meters and the time axis is in seconds.

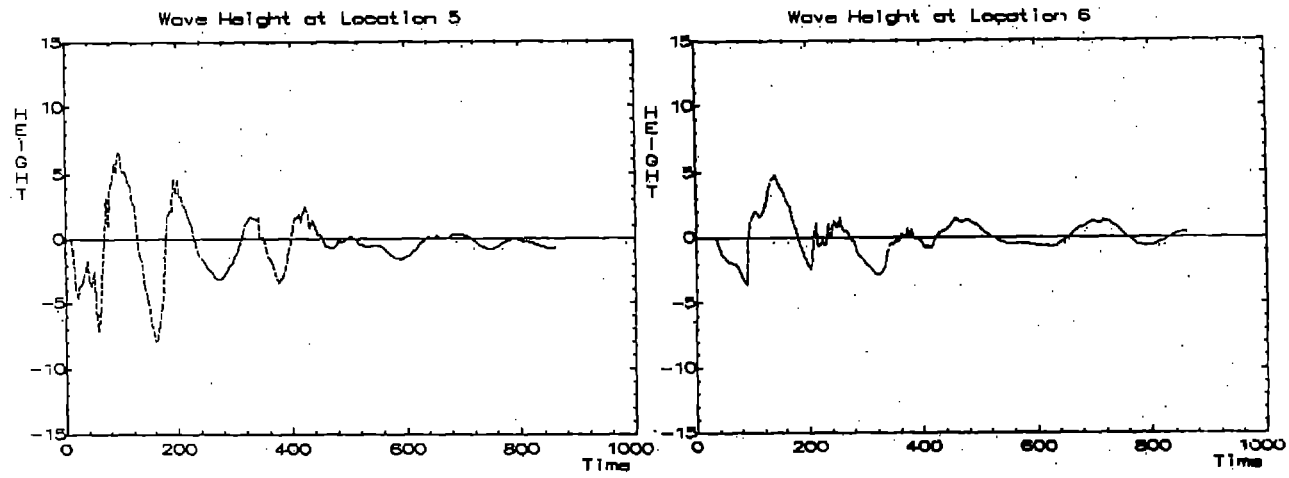

Figure 5. The wave profiles at the south end of the PARN dock (Location 5) and at the tide gauge (Location 6) are shown for the 3 Landslide model. The vertical axis is height in meters and the time axis is in seconds.

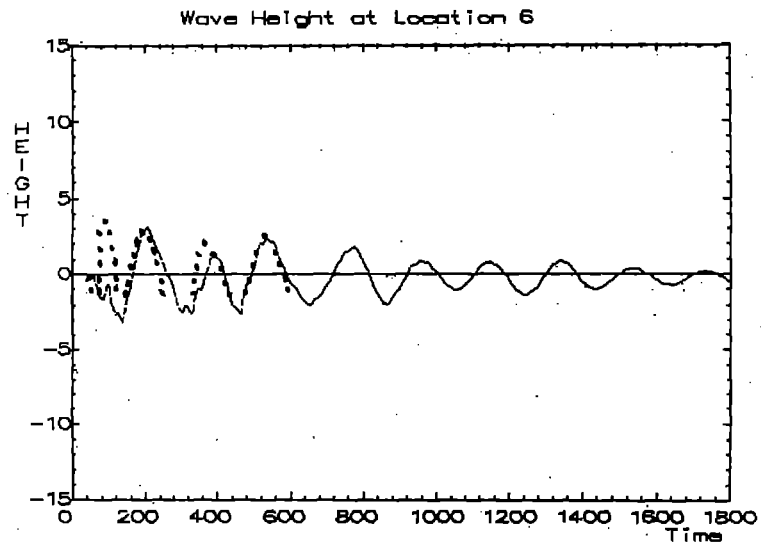

Figure 6. The wave profile at the tide gauge generated by the landslide occurring over a 2 minute interval and the calibrated tide gauge profile (dots). The vertical axis is height in meters and the time axis is in seconds.

INVESTIGATION OF WAVE CHARACTERISTICS INDUCED BY TSUNAMI WAVE ENTERING ENCLOSED WATER AREAS. Mathematical Models, Algorithms, Results of Computational Experiments.*

LEONID B. CHUBAROV, ZINAIDA I. FEDOTOVA, DMITRII A. SHKUROPATSKY

Institute of Computational Technologies,
Siberian Branch of the Russian Academy of Sciences
Lavrentjev Ave. 6, Novosibirsk, 630090, RUSSIA

Abstract

The paper deals with two general problems. First one is the choice and interpretation of approximate hydrodynamical shallow water models, including high order approximations, allowing to take into account nonhydrostatic pressure and weak phase dispersion generated by the vertical flow acceleration. Secondly, the construction of numerical algorithms with given features is investigated providing rather accurate reproduction of nonlinear, dispersive and energy characteristics of the models. Particularly, the construction of implicit finite-difference schemes is also investigated to increase numerical algorithms stability and model continuous nonstationary processes. The presented calculation results were obtained for the water-pool with nearly horizontal bottom and specified flow at boundaries. Free surface elevation and velocities were computed for given locations and times.

Introduction

One of the most sophisticated tsunami phenomena is connected with the processes taking place when the waves come up to the shore, enter the bounded water pools (bays, harbours and other natural and manmade reservoirs) and interact with bottom and coastal relieves.

Many factors affecting the physical phenomena complicate the deduction of proper mathematical models and the construction of numerical algorithms. Well-known problems arise when modelling coastal line motion and wave breakdown. Essentially different time characteristics are also a problem. For example, the time characteristics of wave processes in small water-pools determining the wave propagation entering through the open boundary, the generation of new waves, the coastal interaction and so on are rather less than period of entering waves. Problems of the sort are often arise particularly while modelling tsunami wave entering harbours and interacting with hydro-technical constructions.

The authors investigate the problems through the hierarchy of approximate hydrodynamic models taking into account the following assumption: small slopes of bottom relief, quazi-onedimenionness, prolonged water pools, vertical boundaries. Two general problems are considered. Firstly, choice and interpretation of approximate hydrodynamical shallow water models, including high order approximations, allowing to take into account nonhydrostatic pressure and weak phase dispersion generated by the vertical flow acceleration. Secondly, the construction of numerical algorithms with given features is investigated providing rather accurate reproduction of nonlinear, dispersive and energy characteristics of the models. Particularly, the construction of implicit finite-difference schemes is also investigated to increase numerical algorithms stability and model continuous nonstationary processes.

The authors implied shallow water equations and non-linear dispersive model with one equation with respect to free surface elevation. The finite-difference numerical algorithms were used as well as modified adjustable explicit-implicit Mac-Cormack scheme. The presented calculation results were obtained for the water-pool with nearly horizontal bottom and specified flow at boundaries. Free surface elevation and velocities were computed for given locations and times.

Mathematical models

General formulation

The choice of mathematical models for description of certain physical phenomenon demands preliminary analysis and consideration of inherent features of the phenomenon and comparison of their importance. In particular, the geometry of flow domain for the considered reservoirs (Fig. 1) has dominant direction and their characteristic horizontal scales dominate over the vertical ones. Another parameter is the characteristic time of wave processes.

The coast profile also effects on dynamics of shore line. The influence of bottom friction and surface ice is not so evident.

Shallow water equations

The above-mentioned relevance of water pool scales as well as essential nonlinearity of the wave processes make it possible to investigate the hydrophysical processes in the frameworks of shallow water equations:

$$\begin{aligned} u_t + uu_x + vu_y + g\eta_x &= f_1 , \\ v_t + uv_x + vv_y + g\eta_y &= f_2 , \\ \eta_t + (uh)_x + (vh)_y &= f_3 , \end{aligned} \qquad (1)$$

where u,v are the horizontal velocity components, $h=H+\eta$ is the total depth, H is the undisturbed water depth, η is the free surface elevation, g is the acceleration of gravity. Right parts f_i in motion equations contain the terms describing outer effect (Coriolis force, bottom and wind friction):

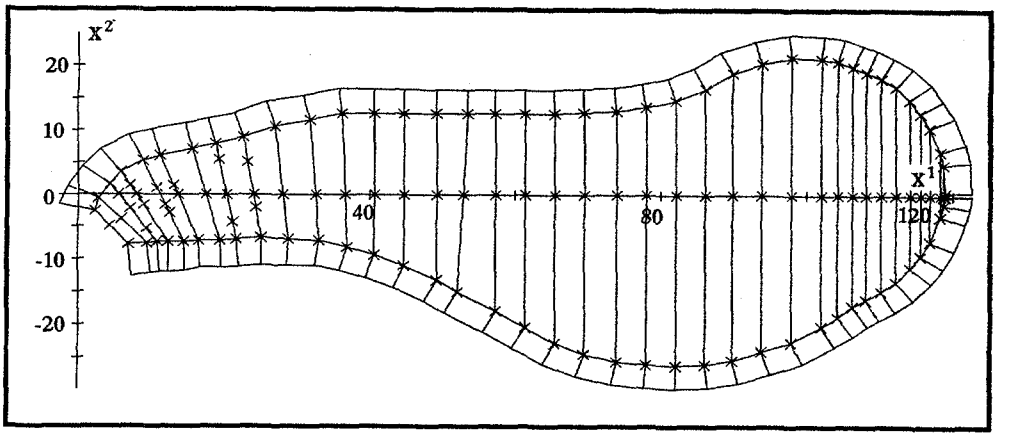

Fig. 1. Characteristic geometry of considered reservoirs.

$$f_1 = lv - g\frac{u\sqrt{u^2+v^2}}{C^2h} + \nu\left(u_{xx}+u_{yy}\right) + f^{(x)},\quad f_2 = -lu - g\frac{v\sqrt{u^2+v^2}}{C^2h} + \nu\left(v_{xx}+v_{yy}\right) + f^{(y)},$$

$l = 2\omega\sin\varphi$, ω is the angle velocity of Earth rotation, φ is the latitude, C - Shezi coefficient determined from relation $C = \frac{R^{1/6}}{n}$ (Manning formula), R is the hydraulic radius usually assumed to be equal to depth H, n is the group friction coefficient, ν is the dynamic viscosity coefficient, $f^{(x)}, f^{(y)}$ are the terms describing wind friction, f_3 is the right part of discontinuity equation describing outer mass sources.

There is another form of the equations preferred when modelling discontinuous fields (propagation of hydraulic shock when dam break-up):

$$\mathbf{T}_t + \mathbf{D}_x + \mathbf{E}_y = \mathbf{F}, \tag{2}$$

where $\mathbf{T} = \{U,V,h\}$, $\mathbf{D} = \left\{\frac{U^2}{h} + g\frac{h^2}{2}, \frac{UV}{h}, U\right\}$, $\mathbf{E} = \left\{\frac{UV}{h}, \frac{V^2}{h} + g\frac{h^2}{2}, V\right\}$,

$$\mathbf{F} = \left\{ghH_x + lV - g\frac{U\left(U^2+V^2\right)}{C^2h^2} + A_1,\quad ghH_y - lU - g\frac{V\left(U^2+V^2\right)}{C^2h^2} + A_2,\quad 0\right\},$$

$$\mathbf{A} = \{A_1, A_2\} = \nu\Delta\mathbf{U} - \nu\mathbf{U}\frac{\Delta h}{h} - \nu\left(\nabla\frac{\mathbf{U}}{h}\right)\cdot\nabla h,\qquad \mathbf{U} = \{U,V\},\ U = hu,\ V = hv.$$

Boundary $\Gamma(t)$ of the flow domain $\Omega(t)$ consists of two parts. One of them $\Gamma_1(t)$ corresponds to water pool entrance at which the flow $Q(t)$ of incoming wave is specified. The other $\Gamma_2(t)$ corresponds to shore line depending on modelling accuracy. It is described as vertical or slope surfaces. Different ways of boundary conditions construction are described in [1]-[4].

St. Venant model

Note that the mentioned water pool prolongness makes 1D shallow water model [5] to be rather accurate for preliminary calculations as well as St. Venant model. St. Venant equations take higher place in hierarchy of approximate hydrodynamic models. They allow to take into account width variation in 1D case.

Accurate deduction of St. Venant equations and corresponding discussion of assumptions and simplification are described by Abbott [6] and Grushevsky [7].

Here are the basic assumptions:

- the transverse velocity component much smaller than the longitudinal one, the centrifugal effects due to curviness is ignored;
- the bottom slope is small;
- friction forces coincide with the ones for shallow water equations; the total effect of friction and rotation is assumed to be described by some friction term.

For these assumptions St. Venant equations can be written as:

$$\begin{aligned} &\frac{\partial Q}{\partial t} + \frac{\partial}{\partial x}\left(\alpha \frac{Q^2}{S}\right) + gS\frac{\partial \eta}{\partial x} + g\frac{Q|Q|}{C^2 SR} - vq\cos\varphi = 0, \\ &\frac{\partial S}{\partial t} + \frac{\partial Q}{\partial x} = q, \end{aligned} \tag{3}$$

where $S = \int_B h' dy$ is the total cross-section square, $Q = \int_B h'\bar{u} dy = \bar{u}S$ is the flow, h' is the local total depth, $\bar{u}$ is the averaged velocity, y is the transverse horizontal coordinate, B is the width of a channel cross-section, q is the boundary income directed at the angle φ to flow lines, v is its mean velocity, $\alpha = \frac{S}{Q^2}\int_S u^2 dS$ is the coefficient of velocity distribution for cross-section (Boussinesq coefficient, usually assumed to be equal to 1), $\eta = \frac{S}{B} - H$, $R = \frac{1}{S}\int_0^B ff(h')^{3/2} ds_y$ is the corrected relation for hydraulic radius R, where ff is the relation of Shezi coefficient in considered cross-section and in the main channel. As told above R is assumed to be equal to H.

Nonlinear-dispersive model

Let consider models taking into account wave dispersion. Both on the base of theoretical investigation and practical experience in the domain of application of approximate hydrodynamic models the classification is accepted, in which the main parameters determining a flow character are the following ones:

$$\alpha = \eta_0/H_0, \quad \beta = (H_0/L)^2, \quad Ur = \alpha/\beta,$$

where η_0 is the characteristic wave amplitude, H_0 is the characteristic depth of a undisturbed water pool, L is the characteristic wave length, α and β are called by parameters of nonlinearity and dispersion, respectively, Ur is the Ursell parameter.

The classification table can be represented in the form:

	Models	*The relations between α and β*
1.	Linear shallow water equations	$\alpha = o(1)$, $\beta = o(1)$,
2.	Nonlinear shallow water equations	$\alpha = O(1)$, $Ur = \alpha/\beta >> O(1)$
3.	Boussinesq type linear equations	$\alpha = o(1)$, $Ur = \alpha/\beta << O(1)$
4.	Boussinesq type nonlinear equations	$Ur = \alpha/\beta = O(1)$

Let consider a certain nonlinearly dispersive model, which is the second order in time equation for the free surface elevation $\eta = \eta(x,y,t)$ [14, 15]:

$$\underbrace{\eta_{tt}}_{A} - \underbrace{g\nabla\cdot\left(H\nabla\eta\right)}_{B} = \underbrace{-l^2\eta}_{C} + \underbrace{\frac{1}{3}\nabla\cdot\left(H\nabla\left(H\eta_{tt}\right)\right)}_{D} + \underbrace{\frac{3}{2}g\nabla\cdot\left(H\nabla\left(\eta^2/H\right)\right)}_{E}. \tag{4}$$

All notations for hydrodynamic variables are determined above, $\nabla = \left(\partial/\partial x, \partial/\partial y\right)$ is the operator vector gradient. This equation can be derived from a variational principle for waves propagating mainly in one direction under the following assumptions:

- long waves flow,
- $\left|\nabla^n H\right| = O(\beta)$, $n = 1,2,\ldots$ – small bottom slope,
- $Ur = \alpha/\beta = O(1)$.

When amplitudes of waves are very small under $\beta < 0.004$ ($L>50H_0$) to describe flow motion one needs to use members *A* and *B*. Such waves travel without dispersion and the wave equation is applied to described them:

$$\eta_{tt} - g\nabla\cdot\left(H\nabla\eta\right) = 0.$$

All terms in the right part of (4) are responsible for dispersion effects. The term *C* represents the Earth rotation. The linear equation of the form:

$$\eta_{tt} - g\nabla\cdot\left(H\nabla\eta\right) = -l^2\eta,$$

giving the relationship between members *A*, *B* and *C* describes propagation of very long waves with a small amplitude for which the Coriolis acceleration products a week dispersion.

For the waves with lengths of the order 5÷50 times of depth the week phase dispersion is produced by vertical acceleration of the flow. For this effect the term *D* is responsible and the corresponding equation of the form

$$\eta_{tt} - g\nabla\cdot\left(H\nabla\eta\right) = -l^2\eta + \frac{1}{3}\nabla\cdot\left(H\nabla\left(H\eta_{tt}\right)\right)$$

is the linear dispersive equation of the Boussinesq type.

Influence of nonlinearity (amplitude dispersion) is described by the term *E*. In the model the formulae for this term is obtained under assumption about quasi one-dimensional wave propagation in the water at rest under the bottom of week slope.

The model

$$\eta_{tt} - g\nabla\cdot\left(H\nabla\eta\right) = -l^2\eta + \frac{3}{2}g\nabla\cdot\left(H\nabla\left(\eta^2/H\right)\right)$$

does not take into account the phase dispersion and can be derived immediately from shallow water equation under above assumption.

Among properties of the equation (4) let mark, that for $l=0$ it has the analytical solution of soliton type

$$\eta = \eta_0\operatorname{sech}^2\left(K^{1/2}\left(x - Ut\right)\right),\quad K = \frac{3\eta_0}{4H_0^2\left(H_0+\eta_0\right)},\quad U = \pm\left(g\left(H_0+\eta_0\right)\right)^{1/2}.$$

The linear analogous of the equation (4) in the one-dimensional case under $H(x)=H_0$

$$\eta_{tt} - c_0\eta_{xx} = \frac{H_0^2}{3}\beta\eta_{xxtt}$$

has the following dispersive relation:

$$\omega^2 = \frac{k^2}{1+\beta k^2/3}.$$

It is seen that for small k, corresponding to long waves the expression for ω

$$\omega = \pm k\left(1 - \beta k^2/6\right) + O\left(k^4\right)$$

coincides by the accuracy of $O(k^4)$ with the one for the linear equation, describing potential flow of nonviscous incompressible fluid in the field of gravity.

Numerical algorithms

To apply both high-performance and high-accuracy algorithms appropriate for the simulation of slow processes within long time is one of the principal questions. According to that implicit (partially implicit) finite-difference schemes on moving adaptive grids are intended to use for approximation of equations (1) and their modifications. At the time explicit schemes on static uniform and nonuniform grids will be used to model fast processes (as the above-mentioned transformation of the hydraulic shock).

The numerical algorithms intended for the realization of the described models regarding respective model calculations are considered mainly in 1D case. Some aspects of 2D realization will be mentioned.

The Godunov scheme for the shallow water equations

The shallow water equation without external factors can be written in a conservative form as follows:

$$\mathbf{T}_t + \mathbf{D}_x = \mathbf{F},\ \mathbf{T} = \{U, h\},\ \mathbf{D} = \left\{\frac{U^2}{h} + g\frac{h^2}{2},\ U\right\},\ \mathbf{F} = \{ghH_x, 0\},\ U = hu. \tag{5a}$$

One of the most effective two-step finite-difference schemes is the explicit Godunov scheme of predictor-corrector type [9] with adaptive approximation viscosity. Then a nonconservative form of the equations is approximated at the first step:

$$\mathbf{U}_t + \mathbf{A}\mathbf{U}_x = \mathbf{F},\ \mathbf{U} = \begin{Bmatrix} u \\ h \end{Bmatrix},\ \mathbf{A} = \begin{pmatrix} u & g \\ h & u \end{pmatrix},\ \mathbf{F} = \begin{pmatrix} gH_x \\ 0 \end{pmatrix}. \tag{5б}$$

On an unmoving uniform grid we have for the scheme:

Predictor:

$$\frac{\mathbf{U}_j - \frac{1}{2}\left(\mathbf{U}^n_{j+\frac{1}{2}} + \mathbf{U}^n_{j-\frac{1}{2}}\right)}{\omega^n_j \tau_n} + \frac{1}{2}\left(\mathbf{A}^n_{j+\frac{1}{2}} + \mathbf{A}^n_{j-\frac{1}{2}}\right)\frac{\mathbf{U}^n_{j+\frac{1}{2}} - \mathbf{U}^n_{j-\frac{1}{2}}}{\Delta x} = \mathbf{F}_j,\ j = 2, \ldots, N-1, \tag{6a}$$

Corrector:

$$\frac{\mathbf{U}^{n+1}_{j+\frac{1}{2}} - \mathbf{U}^n_{j+\frac{1}{2}}}{\tau_n} + \frac{\mathbf{D}_{j+1} - \mathbf{D}_j}{\Delta x} = \mathbf{F}_{j+\frac{1}{2}},\ j = 1, \ldots, N-1. \tag{6б}$$

The implicit Godunov scheme of predictor-corrector type [9] that require to solve matrix three-diagonal equations was also considered as well as the implicit and explicit Mac-Cormack schemes [10]. The implicit Mac-Cormack scheme derived from the explicit one by introducing stabilizing term when locale stability is broken. The "running calculation" algorithm is used for the scheme.

The Godunov scheme for the St. Venant model

For the St. Venant model the same numerical algorithms were used. As in the previous case the finite-difference scheme is based on simplified origin differential equations (3) without external forces and sources.

Predictor:

$$\mathbf{U}_t + \mathbf{A}\mathbf{U}_x = \mathbf{F}\,,\ \mathbf{U} = \begin{Bmatrix} Q \\ S \end{Bmatrix},\ \mathbf{A} = \begin{pmatrix} \dfrac{2Q}{S} & -\left(\dfrac{Q}{S}\right)^2 \\ 1 & 0 \end{pmatrix},\ \mathbf{F} = \begin{Bmatrix} -gS\eta_x \\ 0 \end{Bmatrix}$$

$$\frac{\mathbf{U}_j - \mathbf{U}_j^n}{\omega_j^n \tau_n} + \mathbf{A}_j^n \frac{\mathbf{U}^n_{j+\frac{1}{2}} - \mathbf{U}^n_{j-\frac{1}{2}}}{\Delta x} = \mathbf{F}_j^n\,, \tag{7a}$$

where

$$f_j^n = \frac{1}{2}\left(f^n_{j+\frac{1}{2}} + f^n_{j-\frac{1}{2}}\right),\ \mathbf{F}_j^n = \begin{Bmatrix} -gS_j^n \dfrac{\eta^n_{j+\frac{1}{2}} - \eta^n_{j-\frac{1}{2}}}{\Delta x} \\ 0 \end{Bmatrix},\ j = 2,\ldots,N-1.$$

Corrector:

$$\mathbf{U}_t + \mathbf{D}_x = \mathbf{F}\,,\ \mathbf{D} = \begin{Bmatrix} \dfrac{Q^2}{S} \\ Q \end{Bmatrix},$$

$$\frac{\mathbf{U}^{n+1}_{j+\frac{1}{2}} - \mathbf{U}^n_{j+\frac{1}{2}}}{\tau_n} + \frac{\mathbf{D}_{j+1} - \mathbf{D}_j}{\Delta x} = \mathbf{F}_{j+\frac{1}{2}}\,, \tag{7б}$$

where

$$\mathbf{F}_{j+\frac{1}{2}} = \begin{Bmatrix} -gS_{j+1/2} \dfrac{\eta_{j+1} - \eta_j}{\Delta x} \\ 0 \end{Bmatrix},\ S_{j+\frac{1}{2}} = \frac{1}{2}\left(S_{j+1} + S_j\right),\ j = 1,\ldots,N-1$$

Schemes for 2D case are considered in detail in [11]. A series of 1D equations should be solved in this case for the simplicity of realization.

Numerical algorithm for Boussinesq type equation

Let construct a difference scheme for the equation (4), represented in the following form

$$\varsigma_{tt} = g\nabla\cdot\left(H\nabla\eta\right) - l^2\eta + \frac{3}{2}\nabla\cdot\left(H\nabla\left(\eta^2/H\right)\right), \qquad \varsigma = \eta - \frac{1}{3}\nabla\cdot\left(H\nabla(H\eta)\right).$$

Let approximate this equation by the difference scheme of second order [15]:

$$\begin{aligned}\frac{\Delta_t^1\Delta_t^{-1}}{(\Delta t)^2}\varsigma^n_{jm} = {} & -l^2\eta^n_{jm} + g\frac{\Delta_x^1}{(\Delta x)^2}\left(\mu_x H_{jm}\Delta_x^{-1}\eta^n_{jm}\right) + g\frac{\Delta_y^1}{(\Delta y)^2}\left(\mu_y H_{jm}\Delta_y^{-1}\eta^n_{jm}\right) \\ & + \frac{3}{2}\frac{\Delta_x^1}{(\Delta x)^2}\left(\mu_x H_{jm}\Delta_x^{-1}\frac{\left(\eta^n_{jm}\right)^2}{H_{jm}}\right) + \frac{3}{2}\frac{\Delta_y^1}{(\Delta y)^2}\left(\mu_y H_{jm}\Delta_y^{-1}\frac{\left(\eta^n_{jm}\right)^2}{H_{jm}}\right),\end{aligned} \tag{8a}$$

$$\varsigma^{n+1}_{jm} = \eta^{n+1}_{jm} - \frac{\Delta_x^1}{3(\Delta x)^2}\left(\mu_x H_{jm}\Delta_x^{-1}\left(H_{jm}\eta^{n+1}_{jm}\right)\right) - \frac{\Delta_y^1}{3(\Delta y)^2}\left(\mu_y H_{jm}\Delta_y^{-1}\left(H_{jm}\eta^{n+1}_{jm}\right)\right), \tag{8b}$$

where the following operators are defined for any function ϕ:

$$\Delta_x^1\phi_{jm}^n = \phi_{j+1,m}^n - \phi_{jm}^n,\quad \Delta_x^{-1}\phi_{jm}^n = \phi_{jm}^n - \phi_{j-1,m}^n,\quad \mu_x\phi_{jm}^n = \frac{1}{2}\left(\phi_{j+1,m}^n + \phi_{jm}^n\right),$$

the operators Δ_y^1, Δ_y^{-1}, Δ_t^1, Δ_t^{-1}, μ_y are determined analogously; Δx, Δy, Δt, are grid steps, *j,m,n* are numbers of internal grid nodes.

The way of realization of this difference scheme in such: at first from the equation (8a) we find ς_{jm}^{n+1} and then from the equation (8b), which approximates an elliptic equation with a calculated left part ς_{jm}^{n+1}, we define η_{jm}^{n+1}.

As the difference scheme (8) is a three layer scheme, we need a formulae to calculate ς_{jm}^1, η_{jm}^1.

For this we take a continuity equation in the form $\eta_t = -\nabla\cdot\left((H+\eta)\mathbf{u}\right)$.

When initial distributions of η and $\mathbf{u}$ are known then η_{jm}^1 is calculated by the above equation under known η_{jm}^0, $\mathbf{u}_{jm}^0$, with the help of an explicit two layer scheme, and after that ς_{jm}^1 is found according to the difference approximation of the relation

$$\varsigma = \eta - \frac{1}{3}\nabla\cdot\left(H\nabla\left(H\eta\right)\right).$$

Dispersive analysis of finite-difference schemes

It is well known that the dissipative and dispersive analysis of difference schemes is useful both in explaining the numerical effects in the calculations by the familiar difference schemes and in constructing new difference methods [16, 17].

The idea of this analysis is to compare the properties of solutions of the form

$$\phi(\mathbf{x},t) = Ae^{i(k\mathbf{x}-\omega t)} \tag{9}$$

for difference schemes and for the approximated differential equations with the initial date $\phi(\mathbf{x},0) = \phi_0(\mathbf{x}) = Ae^{i\mathbf{k}\mathbf{x}}$, $|\mathbf{x}| < \infty$, where A is the amplitude, $\mathbf{k}$ is the wave number, ω is the frequency.

The analysis of the dissipative and dispersive properties of a difference scheme is of great practical value, because it allows to consider the scheme as an independent model at the finite steps of a difference grid.

Let consider the quantity Ω:

$$\Omega = e^{-i\omega\Delta t} = \frac{\phi(\mathbf{x},t+\Delta t)}{\phi(\mathbf{x},t)} = |\Omega|e^{i\Phi},\ \text{where } \Phi = \arg\Omega, \tag{10}$$

were the function $\phi(\mathbf{x},t)$ is a solution of an equation of the form (9). It is called the transfer factor. For considered equations $|\Omega| \equiv 1$, $\Phi = \arg\Omega = -\omega\Delta t$ corresponds to the phase shift of the solution of the form (9) in time Δt.

By analogy with (10) we define the transfer factor of a difference scheme:

$$\rho = \frac{\phi(\mathbf{x}_j, t_n + \Delta t)}{\phi(\mathbf{x}_j, t_n)},$$

where $\phi(\mathbf{x}_j, t_n)$ is a grid solution of a difference scheme, Δt is a time interval, $\mathbf{j}$, n are the numbers of grid nodes. The expression for ρ is defined by the difference scheme.

We represent ρ in the form $\rho = \mathrm{Re}\,\rho + i\,\mathrm{Im}\,\rho = |\rho|e^{i\Psi}$, where $\Psi = \arg\rho$

Let give two definitions according to [16]. The quantity $\chi = |\Omega| - |\rho|$ is called the dissipation of a difference scheme, and the quantity $\delta = \Psi - \Phi$ is called the phase error of a difference scheme. In the case under study we have $\chi = 1 - |\rho|$, $\delta = \arg\rho - \arg\Omega$.

Let carry out the analysis of the difference scheme (8) for the case of one space variable (only for the simplicity of manipulations). Linearization in the vicinity of $\eta = \eta_0$ =const leads to the following scheme:

$$\frac{\Delta_t^1\Delta_t^{-1}}{(\Delta t)^2}\varsigma_j^n = \lambda^2\frac{\Delta_x^1\Delta_x^{-1}}{(\Delta x)^2}\eta_j^n,\quad \varsigma_j^{n+1} = \eta_j^{n+1} - \frac{\beta H_0^2}{3}\frac{\Delta_x^1\Delta_x^{-1}}{(\Delta x)^2}\eta_j^{n+1},\quad \lambda^2 = g\left(H_0 + \frac{3}{2}\eta_0\right),$$

where the parameter β is inserted to mark terms responsible for dispersion.

The transition factor ρ of the difference scheme satisfies to the quadratic equation

$$\left(1 + \frac{4\beta\sin^2\frac{\xi}{2}}{3(\Delta x)^2}\right)(\rho - 1)^2 = -4\rho r^2\sin^2\frac{\xi}{2},\quad r^2 = \left(\frac{\lambda\Delta t}{\Delta x}\right)^2,\quad \xi = k\Delta x.$$

Let write the above equation in the form $\rho^2 - 2\rho + b^2\rho + 1 = 0$ where

$$b^2 = \frac{4r^2\sin^2\frac{\xi}{2}}{1 + 4\beta\sin^2\frac{\xi}{2}\Big/3(\Delta x)^2}.$$

Its solutions are $\rho_{1,2} = 1 - b^2/2 \pm \sqrt{\left(\left(1 - b^2/2\right)^2 - 1\right)}$.

If $b^2 > 4$ then $|\rho_{1,2}| > 1$ and the linearized difference scheme is unstable in L_2 [16]. If $b^2 \le 4$ then $|\rho_{1,2}| \equiv 1$.

Under $r^2 \le 1 + 4\beta/3\Delta x^2$ inequality $b^2 \le 4$ is fulfilled, so the condition above can be considered as a sufficient stability condition for the linearized variant of the difference scheme investigated.

Note that the difference scheme (8) contains both physical (model) dispersion, which is defined by parameter β, and the "scheme" one, which owes its origin to the approximation of any terms on the finite grid.

Let investigate the relation between both of this types of dispersion. For this let expand the quantity

$$\Psi = \arg\rho = \operatorname{arctg}\frac{\operatorname{Im}\rho}{\operatorname{Re}\rho} = \operatorname{arctg}\frac{b\sqrt{1 - b^2/4}}{1 - b^2/2} = \operatorname{arctg}(z)$$

in a neighbourhood of ξ=0 in a power series of ξ.

Expand the expression z in a power series of b (b~ξ): $z = b\left(1 + 3b^2/8\right) + O\left(b^4\right)$.

After expanding b in a power series of ξ: $b = r\left(\xi - \xi^3/24 - \beta\xi^3\Big/\left(12(\Delta x)^2\right)\right) + O\left(\xi^4\right)$ we will get finally the formulae for Ψ:

$$\Psi = r\xi - r\frac{\xi^3}{24}\left(r^2 - 1 - \frac{4\beta}{(\Delta x)^2}\right) + O\left(\xi^4\right). \qquad (11)$$

Let denote $\nu_1 = r^2 - 1$, $\nu_2 = \beta/(\Delta x)^2$. In the formulae (11) the quantities of ν_1 and ν_2 are responsible for the "scheme" dispersion and the physical one, respectively. Then in order for the model dispersion to dominate over the "scheme" dispersion it is necessary to hold inequality $\nu_2 > \nu_1$, which implies the relation $(\Delta x)^2$, $(\Delta t)^2 << \beta$.

In addition let denote that the restriction in time step is more week than analogous one for wave hyperbolic equation.

Using above finite-difference algorithms a number of numerical experiments have been carried out, which showed its practical applicability [15].

Computational grids

The construction of grids is considered below. The coordinates of gridpoints in 2D case are computed from the following system of nonlinear equations [18]:

$$\frac{\partial}{\partial q^1}\left(wg_{22}\frac{\partial x^\alpha}{\partial q^1}\right) + \frac{\partial}{\partial q^2}\left(wg_{11}\frac{\partial x^\alpha}{\partial q^2}\right) = 0, \quad \alpha = 1,2, \tag{12}$$

where w is the control function depending on bottom relief H, free surface elevation η and their gradients ∇H and $\nabla\eta$,

$$g_{\alpha\alpha} = \frac{\partial x}{\partial q^\alpha}\frac{\partial x}{\partial q^\alpha} + \frac{\partial y}{\partial q^\alpha}\frac{\partial y}{\partial q^\alpha}.$$

The constructed grid is curvilinear adapting to domain boundaries and quasi-orthogonal. A moving concentration of grid points at wave front can be obtained with the choice of function $w(x,y)$ in form of $w = 1 + \alpha_w|\nabla\eta|$. Such a selective grid density increases accuracy and allows to obtain adequate results with less amount of grid points.

For the 1D case a grid is obtained from an equation similar to (12). In this paper static nonuniform grids are used. Grid points coordinates are obtained from the following finite-difference scheme [18]:

$$\frac{x_i^{n+1} - x_i^n}{\tau} = w^n_{i+\frac{1}{2}}\left(x_{i+1}^n - x_i^n\right) + w^n_{i-\frac{1}{2}}\left(x_i^n - x_{i-1}^n\right), \tag{13}$$

where τ is the iteration parameter.

Boundary conditions

When modelling 1D flows the second boundary condition for a vertical wall is determined from the first boundary condition $u|_{x=L} = 0$ and differential equations (1) $\eta_x|_{x=L} = 0$.

For a slope coast the shore line $x = L(t)$ moves along the wall as described above $\frac{dx}{dt} = u|_{x=L(t)}$.

In a moving coordinate system the point $x = L(t)$ is mapped into point $q = 1$ for the static coordinate system in which boundary conditions are calculated. They are derived from boundary condition $h = 0$ (h is the total depth) and a consequence of the source equations:

$$\left(u_t + \frac{\eta_q}{J}\right)\Big|_{q=1} = 0, \tag{14}$$

to compute $u|_{q=1}$ for calculating the new position of shore line through the second boundary condition of the source differential equations

$$\left(\frac{dx}{dt} = u\right)\Big|_{q=1}. \qquad (15)$$

At the entrance the boundary condition is determined by the flow rate $Q(t)$. Note that the flow has precritic character. So only one boundary condition is necessary. The other one is found by numerical integration on outcoming characteristics.

When solving 2D (plane) problems boundary conditions are also determined from the nonpenetrable condition and the source differential equations for normal to boundary derivative of free surface elevation η [11]. The relations for 2D case are similar to (14) and (15). The shore line is determined parametrically from the equations which are analogous to (15).

Test and model calculations

First of all, the described calculation are intended to verify different numerical algorithms on the given class of problems. Secondly, the preliminary estimation of the flow in the investigated water pool were made. Both existing algorithms used earlier for solving other problems of wave hydrodynamics including modelling of tsunami wave transformation in ocean and at the shore and new ones designed for the problem were implemented.

Test calculations

The linear model of shallow water equations is investigated at first. The transformation of initial cosine-like disturbation in still liquid was numerically modelled:

$$h(x,0) = \begin{cases} 1 + \cos(\pi x / 4), & |x| \le 2 \\ 1, & |x| > 2 \end{cases}, \quad u(x,0) = 0 .$$

The results of three implicit finite-difference schemes (Mac-Cormack, Godunov, Crank-Nicolson [12]) and their explicit analogs (Mac-Cormack, Godunov) are compared. The obtained values of free surface elevation and velocities (Fig. 2) with comparison to theoretical solution showed Godunov and Crank-Nicolson schemes to provide good accuracy even for rather high Curant numbers. The influence of different approximation viscosity ω and smoothing parameters α on scheme properties are investigated for the problem. The determined optimum values $\alpha = 0.5$ and $\omega = 0.6 \div 0.7$ are found to be suitable for solving nonlinear problems considered below.

The classic problem of dam break-up with theoretical solution for the even bottom [13]:

$$h(x,0) = \begin{cases} h_0, x \ge 0, \\ 0, x < 0, \end{cases} \quad u(x,0) = 0,$$

$$h(x,t) = \frac{1}{9g}\left(\frac{x}{t} + 2c_0\right)^2, \quad u(x,t) = \frac{2}{3}\left(\frac{x}{t} - c_0\right), \quad c_0 = \sqrt{gh_0} \qquad (16)$$

was solved in the frameworks of the shallow water model.

The thin water layer with depth $\varepsilon = \delta h_0$ where $\delta \approx 0.001$ and h_0 is the initial water level beyond the dam was substituted for dry bottom in the numerical realization. Explicit and implicit Mac-Cormak and Godunov schemes of predictor-corrector type were used.

Figure 3 shows the implicit and explicit Godunov schemes to be more preferable than the respective Mac-Cormack schemes.

It should be noted that shock wave appears in numerical modelling in terms of "velocity - total depth" for any δ. The "total depth - water flow" approach allows to avoid this effect if parameter ω is appropriate. However, this effect emerges for high Curant numbers and forego the scheme nonlinear unstability.

The mentioned implicit schemes do not allow to obtain satisfactory accuracy with high Curant numbers for the description of break-up. To solve this problem more sophisticated monotonous implicit schemes of higher approximation order should be applied. However, simple schemes can be used for the preliminary estimation.

Model calculations

The results of laboratory experiments (V. Kh. Davletshin) for the investigated water pool showed that main processes occurring in the water pool have 2D character and are determined by depth variation and sophisticated boundary geometry.

Rather nontrivial picture shows at least three critical run-up zones. They are the left boundary of narrow zone, the entry zone and the right boundary of the water pool.

The next considered problem is connected with modelling of the flow when a long wave of a water level rise or a lowering long wave enters the pool. 1D calculations were made in the frameworks of nonlinear shallow water equations and St. Venant equations. The same numerical algorithms were used (scheme (6) for St. Venant model). Initial water level h_0 was the maximum and minimum observed values for low and high water level waves, respectively. Boundary conditions were determined from the flow rate at the entrance.

The calculation results shown on figures 4 and 5 were obtained on uniform grids (with number of nodes $N = 400$). The solid line denotes the initial stage of the processes (wave at the entrance), the dashed line do for the right boundary run-up and the dotted line – for the moment of wave coming back to the entrance. The water pool depth and boundaries are depicted at the top (in meters).

As a result explicit schemes are shown to be suitable for modelling such fast processes as dam break-up. Their realization is rather simple and sufficient accuracy may be obtained.

The results shows that the two models allow to obtain a good quantitative description of the process reproducing the motion of incoming wave front, its interaction with the coast and the propagation of reflected wave. However, quasi-two-dimensionness of St. Venant model allows to take into account nonuniform water pool width.

The figures show that the water level and velocities in the narrow passage of the water pool for the St. Venant model exceed respective values for the shallow water model (describing the flow in the water pool of uniform width). Uneven depth cause small oscillations following the wave front.

The results were compared with the calculation made for 2D shallow water equations (Barakhin, Khakimzyanov). A good correspondence of the St. Venant model and the shallow water equations for water pools with varying width is shown on Fig. 6.

The results shows that the two models allow to obtain a good quantitative description of the process reproducing the motion of incoming wave front, its interaction with the coast and the propagation of reflected wave. However, quasi-two-dimensionness of St. Venant model allows to take into account nonuniform water pool width.

The figures show that the water level and velocities in the narrow passage of the water pool for the St. Venant model exceed respective values for the shallow water model (describing the flow in the water pool of uniform width). Uneven depth cause small oscillations following the wave front.

Acknowledgments

The authors thank V. Kh. Davletshin for initiative in the problem solving and fruitful discussions of some its aspects and V. B. Barachnin and G. S. Khakimzyanov for the cooperation in this work and the presentation of some results for the valuable analysis of investigated models and algorithms.

References

1. *Voltzinger N. E., Klevanny K. A., Pelinovsky E. N.* Long wave dynamics of coastal zone. – Leningrad: Hydrometeoizdat, 1989. – 271 pp.
2. *Novikov V. A., Fedotova Z. I., Kuzmicheva T. V. On* some problems in modeling long waves run-up to the shore with sophisticated profile. // Vychislitelnye technologii. – Novosibirsk: ICT SD RAS, 1993, – v. 2, – № 4, – pp. 196-209.
3. *Khakimzyanov G.S.* On boundary conditions of finite-difference scheme for the computation of potential flow of liquids with free surface. // Actualnie problemy sovremennoy matematiki. – Novosibirsk: NII MIOO NGU, 1995, – v. 1, – pp. 164-174.
4. *Barakhnin V. B., Khakimzyanov G. S.* A numerical realization of boundary conditions for the one-dimensional shallow water equations. // Actualnie problemy sovremennoy matematiki. – Novosibirsk: NII MIOO NGU, 1995, – v. 1, – pp. 18 - 30.
5. *Marchuk A. G., Chubarov L. B., Shokin Yu. I.* The numerical modeling of tsunami waves. – Novosibirsk: Nauka, 1983. – 176 pp.
6. *Abbott M. B.* Numerical hydraulics. Hydraulics of the open flow: – M.: Energoatomizdat, 1983. – 272 pp.
7. *Grushevsky M. S.* Nonstationary water motion in revers and channels. – Leningrad: Gidrometeoizdat, 1982. – 284 pp.
8. *Shokin Yu. I., Khakimzyanov G.S.* A finite-difference technique for the computation of for the computation of potential flow of liquids with free surface. // Vychislitelnye technologii. – Novosibirsk: ICT SD RAS, 1992. – v. 1, – № 1, – pp. 154-176.
9. *Godunov S. K., Zabrodin A. B., Ivanov M. Ya., Krayko A. N., Prokopov G. P.* The numerical solution of many-dimensional problems of gas dynamics. – M.: Nauka, Glavnaya redaktsiya phiziko-tekhnocheskoy literatury, 1976. – 400 pp.
10. *MacCormack R. V.* A Numerical Method for Solving the Equations of Compressible Viscous Flow. // AIAA Journal, 1982, – v. 20, – № 9, – pp. 1275-1281.
11. *Barakhnin V. B., Khakimzyanov G. S.* The numerical investigation of maximum run-up of tsunami waves in frameworks of two-dimensional shallow water equations. // - to appear, – p. 9.
12. *Fletcher C. A. J.* Computational Techniques for Fluid Dynamics. Fundamental and General Techiques. – Springer-Verlag, Berlin e.a., 1988. vol.1-2, 504 p.
13. *Stoker J. J.* Water Waves. The Mathematical Theory with Applications. – Interscience publishers Ltd.; New-York – London, 1957. – 618 pp.
14. *Kim K. Y., Reid R. O., Whitaker R. E.* On an open radiational boundary condition for weakly dispersion tsunami waves. // J.Comput.Phys., 1988. V. 76. P. 327-348.
15. *Fedotova Z. I., Novikov V. A.* Numerical modelling of long wave propagation in bays on the base of simplified Boussinesq model. // Proceedings of All-union conference on numerical methods in wave hydrodynamics problems. Krasnoyarsk: Computing Center of Academy Science of the USSR, 1991. -pp. 21-26.
16. *Shokin Yu. I.* The method of differential approximation. // Springer-Verlag, Berlin e.a., 1983, 296 p.
17. *Fedotova Z. I., Pashkova V. Yu.* On the numerical model of the dynamics of the weakly nonlinear waves with dispersion// RJNAMM, 1995, v.10, N 5, pp.407-424.
18. *Khakimzyanov G. S., Shokina N. Yu.* Equidistribution method for generation of two-dimensional adaptive grids. // Vychislitelnye technologii. – Novosibirsk: ICT SD RAS, 1992. – v. 4, – № 13, – pp. 271-282.

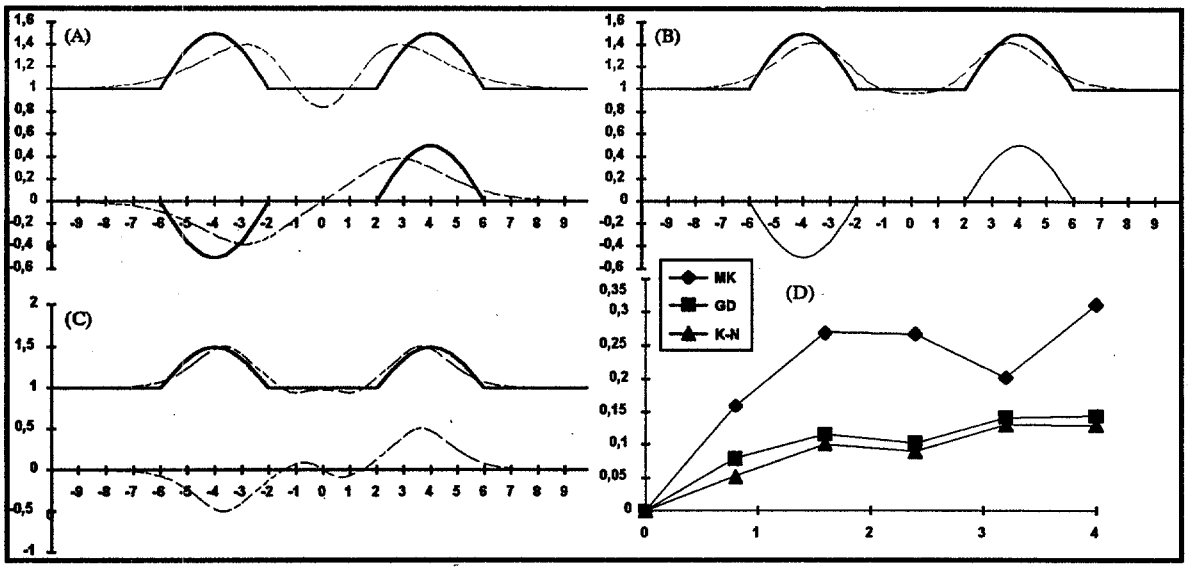

Fig. 2. The comparison of implicit schemes for transformation of initial disturbation. The space pictures of the total depth h (the upper curves) and the flow hu (the lower curves) at time $t = 4$ were obtained for Mac-Cormack (A), Godunov (B) and Crank-Nicolson (C) schemes. The maximum error with respect to time (D) is shown. The following parameters of numerical algorithms were used: smoothing coefficient after *predictor* $\alpha 1 = 0.5$, smoothing coefficient after *corrector* $\alpha 2 = 0.2$, $r \equiv \Delta t/\Delta x = 4.0$, $\Delta x = 0.2$, $\omega = 0.6$.

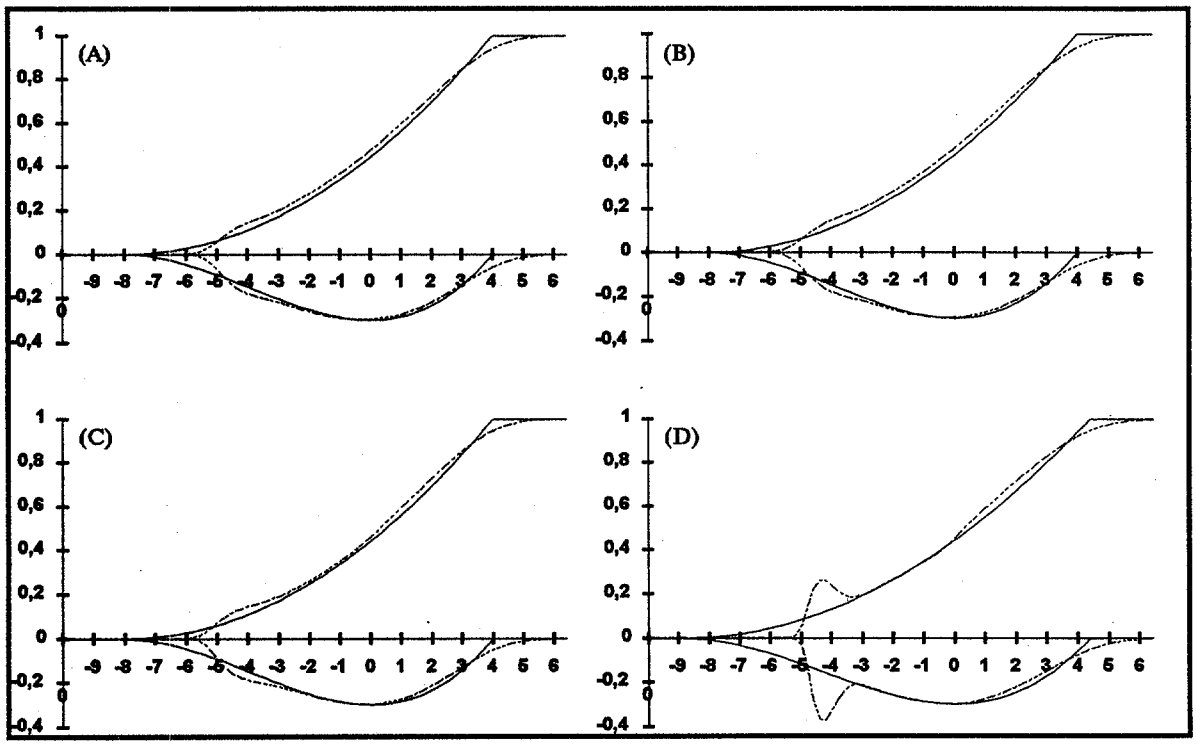

Fig. 3. The comparison of implicit and explicit Godunov schemes for dam break-up problem. Solid line shows the theoretical solution (16). Solutions for the total depth h (the upper curves) and the flow hu (the lower curves) are given at time t=4. The following parameter values were used: $\Delta x = 0.2$, $\omega = 0.6$, smoothing after predictor $\alpha 1 = 0.5$, smoothing after corrector $\alpha 2 = 0.5$, $r \equiv \Delta t/\Delta x = 0.4$ for the explicit scheme (A) and $r = 0.4$ (B), $r = 1.0$ (C) and $r = 2.0$ (D) for the implicit scheme.

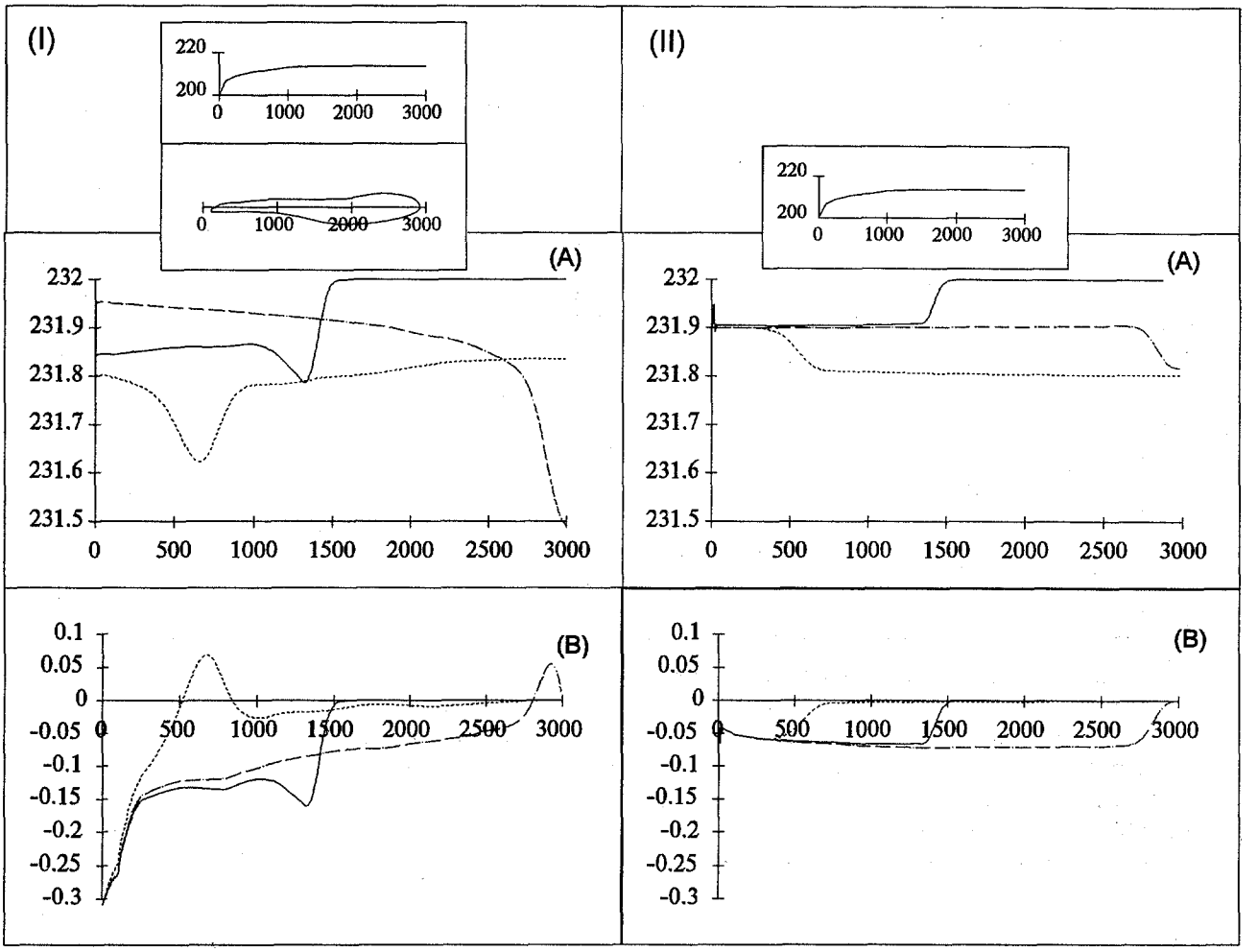

Fig. 5. Free surface (A) and velocity (B) profiles for St. Venant (I) and shallow water model (II) computed at different times are shown for lowering long wave.

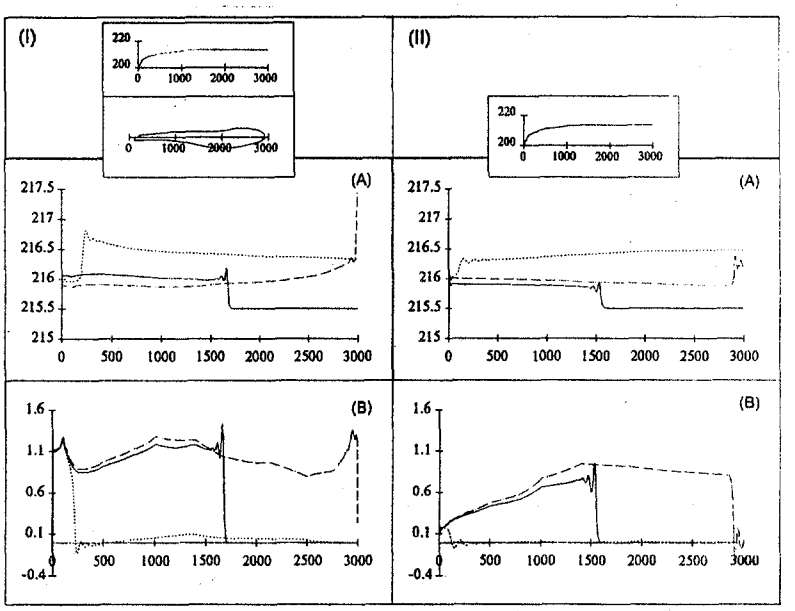

Fig. 4. Free surface (A) and velocity (B) profiles for St. Venant (I) and shallow water model (II) computed at different times are shown for long wave of a water level rise.

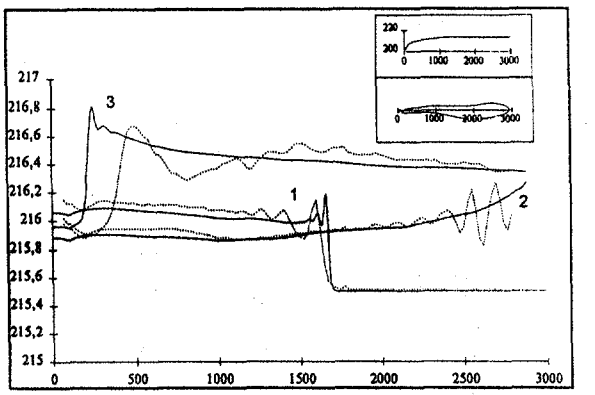

Fig. 6. Water levels for incoming long wave of a water level rise. Results for St. Venant model (solid line) and 2D shallow water equations (averaging on width was made) are shown. The incoming wave at the entrance (1), right boundary run-up (2) and wave coming back to the entrance (3).

APPLICATION FOR MEMBERSHIP

THE TSUNAMI SOCIETY
P. O. Box 25218
Honolulu, Hawaii 96825, USA

I desire admission into the Tsunami Society as: (Check appropriate box.)

☐ Student ☐ Member ☐ Institutional Member

Name _____ Signature _____

Address _____ Phone No. _____

_____

Zip Code _____ Country _____

Employed by _____

Address _____

Title of your position _____

FEE: Student $5.00 Member $25.00 Institution $100.00

Fee includes a subscription to the society journal: SCIENCE OF TSUNAMI HAZARDS.

Send dues for one year with application. Membership shall date from 1 January of the year in which the applicant joins. Membership of an applicant applying on or after October 1 will begin with 1 January of the succeeding calendar year and his first dues payment will be applied to that year.